Nonlinear carbon feedbacks in CMIP6 and their impacts on future freshwater availability

Justin S. Mankin[a,b], Noel Siegert[a,b], Jason E. Smerdon[b,c], Benjamin I. Cook[b,d], Richard Seager[b], A. Park Williams[e], Corey Lesk[a], Zhiying Li[a], Harmanveer Singh[a,f], & Emily Martinez[a]

[a] *Department of Geography, Dartmouth College, Hanover, NH*

[b] *Lamont-Doherty Earth Observatory of Columbia University, Palisades, NY*

[c] *Columbia Climate School, Columbia University, New York, NY*

[d] *NASA Goddard Institute for Space Studies, New York, NY*

[e] *Department of Geography, UCLA, Los Angeles, CA*

[f] *School of Marine & Atmospheric Sciences, Stony Brook University, Stony Brook, NY*

Corresponding author: Justin S. Mankin, mankin@dartmouth.edu

This manuscript has been accepted for publication at Journal of Climate.

ABSTRACT

Some theories and analyses of earlier generations of Earth System Models (ESM) suggest that transpiration will decline with higher atmospheric carbon dioxide concentrations [CO_2] due to stomatal closure, thereby enhancing runoff and soil moisture relative to the continental drying predicted by warming alone. Using the latest generation of idealized experiments from the Coupled Climate-Carbon Cycle Model Intercomparison Project forced with increasing [CO_2], we show that the opposite effect prevails: plants themselves contribute to projected soil drying, with smaller negative effects on runoff, and this picture emerges by considering the interactions between radiatively driven warming and the physiological effects of high [CO_2] on plants. These interactions act to increase plant-based evapotranspiration (ET) by expanding leaf area and lengthening and warming growing seasons beyond what would be predicted by radiative or biogeochemical effects alone. Collectively, these interactions increase ecosystem water use and dry soils, compensating any land water savings from stomatal closure. At the same time, these interactions have grown and become more uncertain across ESM generations. We also find that the simulated strength of these plant-water interactions scale with the resilience of the land carbon sink to warming—a key feedback in the carbon cycle. Our results emphasize that a linearity assumption underpinning analyses of carbon, plant, and water interactions is not appropriate for the latest generation of ESMs, with implications for model development, as well as the accurate interpretation of projected changes to the carbon cycle and the consequences for future climate, drought, and water availability.

SIGNIFICANCE STATEMENT

Understanding plants and how their water use will respond to climate change is essential to understanding future drought and aridity. We demonstrate that interactions between warming and higher atmospheric carbon dioxide in the latest generation of climate models lead to amplified plant growth and associated plant water use. The simulated strength of this interaction is related to weaker land carbon losses from warming. The net result is that in climate models, plant responses forcing enhance land surface drying rather than reduce it, as previous analyses of earlier generations of climate models have found. Our findings highlight that as models become more sophisticated, carbon feedbacks become more uncertain with implications for how we assess plant influences on water cycle changes.

1. Introduction

Plants and their countervailing responses to anthropogenic greenhouse gas emissions and climate change will impact the fate of water availability on land (Idso and Brazel 1984). Some theories, modeling, and nascent observations have suggested that high atmospheric carbon dioxide concentrations (hereafter [CO_2]) reduce plant transpiration, leaving more water for other components of land surface hydrology, like runoff or soil moisture (Idso and Brazel 1984; Swann et al. 2016; Fowler et al. 2019; Roderick et al. 2015; Keenan et al. 2013; Zhou et al. 2023). Earth System Models (ESMs) parameterize plant photosynthesis to capture the real world in which carbon gains are optimized while minimizing water losses (Sabot et al. 2022; Medlyn et al. 2011; Cowan and Farquhar 1977; Bonan et al. 2014). As [CO_2] increases, stomatal conductance declines (Zhang et al. 2018), diminishing the atmosphere's access to deep soil moisture via transpiration (Field et al. 1995) and increasing canopy resistance to evapotranspiration (ET) (Roderick et al. 2015; Milly and Dunne 2016; Lemordant et al. 2018). This leads plants to photosynthesize at a lower water cost under higher [CO_2], manifesting as increased plant water use efficiency (WUE) (Keenan et al. 2013; De Kauwe et al. 2013). Together, such stomatal closure and consequent WUE increases suggest that plant physiological responses to high [CO_2] will "turn on the tap" (Jasechko 2018), meaning they will either directly enhance runoff and soil moisture or reduce the drought and aridity risks projected by the radiative effects of warming alone (Idso and Brazel 1984; Swann et al. 2016; Fowler et al. 2019; Roderick et al. 2015; Betts et al. 2007; Milly and Dunne 2016; Yang et al. 2019; Aston 1984; Lemordant et al. 2018; Scheff et al. 2021).

While prior work emphasizes that plant responses to [CO_2] might enhance land water availability in some regions, other analyses emphasize that total plant-based ET increases in the models, decreasing runoff and soil moisture (Mankin et al. 2018, 2017a, 2019), with implications for water availability (Mankin et al. 2017b) and drought globally (Cook et al. 2021, 2020). In transient simulations, [CO_2]-amplified plant growth due to CO_2 fertilization manifests as increased leaf area (and associated canopy interception and leaf evaporation). Together with longer and warmer growing seasons, plant-based ET can increase, even in the face of enhanced stomatal closure. Some studies have used emergent constraints methods to reduce projection uncertainty in CO_2 fertilization (Cox et al. 2013; Keenan et al. 2023) and its associated hydrologic consequences (Mankin et al. 2019; Lehner et al. 2019). Yet, persistent uncertainties in plant responses to [CO_2] across model generations remain. For example, the

IPCC's Working Group I concluded in the 6th Assessment Report that "there is *low confidence* that increased WUE by vegetation will […] diminish the frequency and severity of soil moisture and streamflow deficits associated with the radiative effect of higher CO_2 concentrations" (Canadell et al., 2021). The U.S. Fifth National Climate Assessment differs from the IPCC conclusion, emphasizing that the remaining uncertainties imply the possibility of plant-induced water savings, stating that "[...] changes in plant water use in response to increasing temperatures and rising atmospheric CO_2 are complex and poorly understood and may either ameliorate or amplify soil moisture and runoff droughts at the surface" (Leung et al. 2023). As such, this important source of uncertainty in projections of future freshwater availability, with the potential to inform drought mitigation and adaptation decisions globally, remains unresolved.

The uncertainty in ecohydrological responses to [CO_2] in models emphasizes the importance of accurately representing the interactions among the carbon, nutrient, and water cycles as expressed through plants. Importantly, biogeochemical sophistication in ESMs has increased considerably across generations (Arora et al. 2020) as land surface models have rapidly developed (Fisher and Koven 2020). Such model advancements have been driven in part by the longstanding recognition that simulating coupled carbon and nutrient cycles could influence nonlinear responses in terrestrial carbon and water budgets. Such responses would likely affect projected warming and climate impacts as well. For example, there is a long history of work focused on how nitrogen (Vitousek and Howarth 1991) can limit plant productivity responses to enhanced [CO_2], with consequences for carbon feedbacks and hydrologic impacts (Sokolov et al. 2008; Zaehle et al. 2010; Zaehle 2013; Zaehle et al. 2015; Thornton et al. 2009; Felzer et al. 2009; Lee et al. 2013; Davies-Barnard et al. 2020).

Recent work has shown that the latest generation of ESMs participating in the sixth phase of the Coupled Model Intercomparison Project (CMIP6) exhibit more sizable interactions among the radiative and biogeochemical effects of [CO_2] than in previous CMIP generations, driven in large part by changes in net primary production (Huang et al. 2022). Here we extend this important work, showing that in the CMIP6, these interactions in carbon responses to warming and high [CO_2] are related to the carbon-climate feedback and generate hydrologic responses with implications for the interpretation of how plants responses to warming and [CO_2] will impact terrestrial water availability.

Using the idealized 1% [CO_2] experiments performed under the CMIP6 Coupled Climate-Carbon Cycle Intercomparison Project (C4MIP) framework (Jones et al. 2016), we present three key findings. Firstly, within the CMIP6, there is a sizable interaction between warming and enhanced [CO_2]. The interaction leads to amplified plant growth, the ensemble variation in the strength of which, we show, is tightly associated with ensemble variation in the response of the atmosphere-land CO_2 flux to warming. Secondly, this amplified plant growth generates an increase in plant-based ET beyond that predicted by radiative or biogeochemical effects individually or their sum, cancelling any transpiration reductions from the stomatal effects of [CO_2] and causing declines in soil water. Lastly, runoff changes within the ensemble are associated with precipitation changes (Lesk et al. 2025), not plant-based ET changes. The causes of interactive terms in the carbon cycle in CMIP6 relative to earlier CMIP generations is a crucial question for future evaluation. Together, our results highlight that while CMIP6 projections of future aridity require reconciling plant responses to [CO_2], doing so provides little evidence that plant stomatal responses will increase future water availability or offset radiatively driven drying. Relative to the present day, these idealized projections suggest increased plant-based ET for much of the globe, with model uncertainties in carbon cycle responses playing a key role in determining broader hydrologic impacts.

2. Data & Methods

a. Climate model experiments

All ESM data used in this study come from a set of experiments conducted as part of CMIP6 (Jones et al. 2016; Friedlingstein et al. 2006), downloaded from the Earth System Grid Federation (https://esgf-node.llnl.gov/search/cmip6/) and analyzed via Python and R.

A common approach to assess whether plants will tend to 'wet' or 'dry' the surface is to compare hydrologic responses in a set of idealized ESM experiments that isolate plant responses to [CO_2] from other factors associated with radiatively driven changes. This protocol was originally developed over 20 years ago (Friedlingstein et al., 2006; Fung et al., 2000) to quantify the strength of carbon feedbacks arising from climate changes versus enhanced [CO_2], and is evaluated using the C4MIP framework, a model intercomparison approved by CMIP6 (Jones et al. 2016). In the idealized experiments used in C4MIP, [CO_2]

148 is quadrupled from its preindustrial level by increasing at a rate of 1% per year for 140 years
149 (i.e., "4xCO2"). The difference among simulations resides in the parts of the model that are
150 allowed to respond to the [CO_2] increase. We use data from 13 models (ACCESS-ESM1.5,
151 BCC-CSM2-MR, CanESM5, CanESM5-CanOE, CESM2, CMCC-ESM2, CNRM-ESM2-1,
152 EC-Earth3-CC, GFDL-ESM4, IPSL-CM6A-LR, MIROC-ES2L, NorESM2-LM, and
153 UKESM1.0-LL) participating in the experiments that contributed results to C4MIP and for
154 which the required variables are available: (1) The 1% CO_2 experiment ("1pctCO2", termed
155 "coupled" or COU), which is a fully coupled simulation forced with an increase in
156 atmospheric CO_2 concentrations of 1% per year for 140 years from preindustrial until
157 quadrupling, conducted as part of the CMIP6 DECK; (2) The 1% [CO_2] biogeochemically
158 coupled run ("1pctCO2-bgc", termed BGC), in which only the land and ocean
159 biogeochemical schemes respond to [CO_2], not the climate; and (3) The 1% CO_2 radiatively
160 coupled run ("1pctCO2-rad", termed RAD), in which only the radiation scheme responds to
161 increasing [CO_2], while the land and ocean biogeochemical schemes are prescribed
162 preindustrial [CO_2] levels. Collectively, the COU, BGC, and RAD experiments allow
163 analyses of how climate and the carbon cycle independently respond to increased [CO_2] and
164 how those responses generate carbon feedbacks from the land and ocean acting to amplify or
165 dampen climate change. We also use results from seven models that participated in C4MIP
166 during the fifth phase of the Coupled Model Intercomparison Project (CMIP5) to compare
167 against results from C4MIP for CMIP6 (bcc-csm1-1, CanESM2, CESM1-BGC, HadGEM2-
168 ES, IPSL-CM5A-LR, MPI-ESM-LR, NorESM1-ME). We note that the net ecosystem
169 exchange variable was not available for CESM1-BGC from CMIP5; we opted to include the
170 model for all analyses that do not rely on that variable.

171 Our effort centers on investigating the linearity of carbon and water terms in the C4MIP,
172 building on earlier work with previous generations of the experiment that focused on their
173 independent effects in the RAD and BGC runs (Swann et al. 2016; Fowler et al. 2019; Zhou
174 et al. 2023). Linearity in the context of the C4MIP means that one can generally recover the
175 fully coupled 1pctCO2 response after the 140-year simulation (ΔCOU) by summing each
176 model's isolated biogeochemical (ΔBGC) and radiative (ΔRAD) responses as $\Delta COU \approx \Delta BGC + \Delta RAD$. Any residual in this calculation, $NL = \Delta COU - (\Delta BGC + \Delta RAD)$, is what
178 we call the "nonlinear term," NL, for any quantity at hand. We investigate the NL terms for
179 carbon, plant, and hydrologic variables to assess how the RAD and BGC schemes in the

models interact to affect the COU response and what that implies about how plants impact water availability.

b. Data processing

Monthly hydrologic variables (precipitation, "pr"; runoff, "mrro"; transpiration, "tran"; leaf evaporation "evspsblveg"; soil evaporation, "evspsblsoi") are converted to monthly totals in mm and then resampled to be water year (WY) totals, which we define as October-September in the Northern Hemisphere and July-June in the Southern Hemisphere.

We preprocess monthly layered soil moisture ("mrsol") from each model, integrating soil moisture in each model to a common 2-m depth in units of mm. Soil moisture is analyzed as a WY average, weighted by the number of days in each month. We also calculate vapor pressure deficit (VPD, kPa). To do so, we use monthly near-surface (2-m) air temperature ("tas") and relative humidity ("hurs") to estimate the saturation vapor pressure (e_s, kPa) as $e_s = 0.61078 \times e^{\frac{17.269\mathrm{T}}{273.3+T}}$, where T is temperature (°C); we calculate VPD as $vpd = (1 - rh/100) * es$, where rh is relative humidity (%), which we aggregate to WY means. Ecosystem-scale water use efficiency (WUE) is calculated as the ratio of gross primary productivity (GPP, "gpp" on ESGF) to transpiration ("tran"). Both of these ratios are calculated at the WY scale. Extreme precipitation, where analyzed, is calculated using daily precipitation for the models and experiments for which it is available, estimating the Rx5d measure, which is the maximum total precipitation (mm) occurring over a five-day period in each WY. Within each WY, we estimate the start of the growing season using two-day rolling mean of daily 2-m temperature to identify frost events as those in which two-day mean temperatures are less than zero. The growing season is then the longest consecutive stretch of days without frosts in each WY. Throughfall is calculated as the difference between WY total precipitation and WY leaf evaporation (E_L), which is the evaporation of intercepted precipitation. Gross primary productivity ("gpp"), leaf area index ("lai"), and the land carbon store quantities (vegetation, "cVeg"; litterfall, "cLitter"; soil, "cSoil") are all resampled to WY averages weighting by days per month, as above.

In all variables except where otherwise noted, WY changes in response to 4xCO2 are calculated as the difference between the average of the last 30 water years and the first 30 water years in each 140-year experiment (e.g., **Figs. S1 and S2**). All quantities are calculated on the native grids for each model and experiment. Where ensemble means are presented, the

change from each model is calculated and then interpolated to a common 1°x1° grid (based on the CESM2 grid). For all data except the carbon cycle data, we mask out grid cells where the ensemble mean climatological monthly peak LAI is below 0.1 m^2/m^2. This masks barren regions like Greenland and the Sahara and other extremely low vegetation areas (shown as grey in maps). For the ensemble mean fields, statistically significant change is calculated at the regridded grid-point scale based on a Kolmogorov-Smirnov (K-S) test. To do this, we pool all model water years from the first and last 30 years of each experiment and test the statistical significance of the difference between them. We mask out (in white) any grid cells where the K-S test indicates little difference between the two periods ($p \geq 0.05$). Where we present regional or global averages, we area-weight the average of each model on their native grids.

c. Carbon cycle feedback calculations

Carbon cycle feedbacks are calculated following previous work using the "BGC-COU" approach (Arora et al. 2020). Where available, we use the [CO_2] time series provided by each model ("co2") or those provided as a data addendum to Arora et al. (2020) or based on the last CO_2 value in the preindustrial control simulation. Where CO_2 data are not archived, we calculate their annual value for year *i* assuming a 1% compounding increase from 285 ppm based on the C4MIP experimental design. Following Arora et al. (2020), for each model and experiment, we calculate the change in the total global land carbon storage (sum of cVeg, cLitter, and cSoil in petagrams of carbon PgC) as the area-weighted average of carbon change at each grid cell. We compute temperature changes based on monthly 2-m temperature for each model and experiment as the temperature change between year 139 and year 0 of the simulation.

We compute the land carbon-concentration feedback, β_L, or what we call β in this analysis, as $\beta = \frac{1}{c'}\left(\frac{\Delta C^* \Delta T' - \Delta C' \Delta T^*}{\Delta T' - \Delta T^*}\right)$, where *c* refers to [$CO_2$] change, ΔC refers to the change in total land carbon stores, ΔT refers to 2-m temperature changes, primes (') refer to quantities from the coupled run (COU) and the asterisks (*) refer to those from the biogeochemical experiment (BGC); the units of β are PgC ppm^{-1}. The carbon-climate feedback over land, or γ_L, which we call γ, is calculated as $\gamma = \frac{\Delta C' - \Delta C^*}{\Delta T' - \Delta T^*}$; the units are PgC $°C^{-1}$. These calculations are performed on global quantities over land.

To estimate net ecosystem exchange (NEE), we follow earlier work (Huang et al., 2022). We calculate the "C_{int}" quantity they present, which is equivalent to the nonlinear term on net ecosystem exchange (NEE) or what we call NEE_{NL}. We calculate time-cumulative net primary productivity ("npp") and heterotrophic respiration ("rh") fluxes for each model and grid cell, estimating the flux in total PgC. In contrast to Huang et al. (2022), and to be consistent with the rest of our analysis, we define the reference carbon flux as the climatological average flux over the first 30 years of the experiment. We remove the reference flux from the integrated time series in each grid cell, model, and experiment and estimate net ecosystem exchange (NEE, also called C by Huang et al. (2022)) as the difference between NPP and heterotrophic respiration; the total change in NEE is simply the value in the last simulation year. We compute the nonlinear term for NEE, called NEE_{NL}, as $NEE_{NL} = \Delta NEE' - (\Delta NEE^{*} + \Delta NEE^{+})$, where, as above, primes signal the COU, asterisks, the BGC, and the plus sign ("+") refers to the RAD simulation. All interactive, or nonlinear terms (i.e., COU – BGC – RAD), which are presented with an "NL" subscript, are calculated similarly as $X_{NL} = \Delta X' - (\Delta X^{*} + \Delta X^{+})$. All model-by-model regressions are linear ordinary least squares (OLS) with the fit and significance (Student's t-test) reported.

d. Hydrologic budget framework

Following earlier work (Mankin et al. 2018, 2019), we use a hydrologic budget that assumes climatological WY precipitation (P) is balanced by plant-based ET, or what we term the "canopy water flux" (C, which is the sum of transpiration and evaporation from the leaf surface, E_L), total runoff (Q, surface and subsurface) fluxes, and soil water (S, which we calculate as the sum of soil evaporation and each year's change in WY mean 2-m soil moisture, calculated as the first difference of the soil moisture time series). Following earlier work, we write this budget as P = C + Q + S, where all terms are WY totals in mm. We note two things: firstly, S can equivalently be represented as the residual of P – C – Q. In fact, a comparison between changes in the S term and the change in the residual from P – C – Q are similar in pattern and magnitude, suggesting that our S term effectively characterizes the residual in the hydrologic budget (**Fig. S3**). Secondly, snow is not explicitly considered in our budget owing to the fact that we analyze climatological WY changes over vegetated regions (recall the LAI mask described in *b. Data Processing*), making any multi-year snowpack exceedingly rare. To ensure this is not an issue and that our budget terms recover model precipitation, we calculate precipitation partitioning to each WY term C, Q, and S as the ratio

of each to WY total precipitation (e.g., for canopy partitioning as C/P). We find that the partitioning ratios sum to unity nearly everywhere outside of High Mountain Asia, suggesting the terms we include in our water balance equation capture the scope of each model's hydrologic budget and reproduce WY total precipitation.

For the regional analyses, we calculate the ensemble mean changes in precipitation partitioning to each budget term, Δ(C/P), Δ(Q/P), and Δ(S/P) in the COU for all grid points by averaging across all models. Based on that ensemble mean response in the COU, we then classify and group all grid points that share positive signed changes in partitioning to runoff, Δ(Q/P), or to plant canopies, Δ(C/P). We then calculate area-weighted averages across all these grid points for a number of quantities to assess the composite response over regions where runoff or canopy partitioning increases as a function of [CO_2]. We use this same approach to calculate ΔP positive versus ΔP negative regions, again, based on the response in the COU. Where time series are presented, we present the 30-year rolling mean as a function of [CO_2]; statistical significance in the time series is presented as a thicker line where the model signal (the ensemble mean change evaluated at that time point) is greater than one standard deviation of the ensemble variability (S/N>1). Where we present grid-point level scatter plots, we construct them by pooling all model grid points on their native grids. To calculate the canopy water flux (C) for the ACCESS-ESM1-5 model, we use C = ET – soil evaporation ("evspsbl" minus "evspsblsoi"), as this model does not provide "tran" or "evspsblveg" to the ESGF archive.

3. Results

Our analysis centers on whether plants will consume more or less water in a high [CO_2] versus low [CO_2] world and what the hydrologic consequences of those plant-water use changes will be. We present our analysis in six parts: (1) we motivate the work by showing the pattern of projected greening and drying in the CMIP6 ensemble, which suggests future plant growth and ecosystem health in the face of land water availability declines; (2) to understand this overlapping greening and drying, we outline the set of radiative versus physiological plant-relevant responses in the CMIP6 C4MIP experiments; (3) we show that there are sizable nonlinear terms in vegetation productivity in the CMIP6 C4MIP experiment, much larger than those in CMIP5, emphasizing that nonlinear interactions among the RAD

and BGC simulations have grown across model generations and act to amplify projected plant growth beyond what would be expected from CO_2 fertilization or temperature effects alone; (4) we show that ensemble variation in nonlinear vegetation growth is closely tied to ensemble variation in the climate-carbon feedback, or γ, a key climate parameter; (5) we use a simple hydrologic framework to show that these vegetation growth nonlinearities emerge from carbon cycle processes and generate positive nonlinearities in plant-based ET; and (6) we show that these increases in plant-based ET from interactive warming and [CO_2] are tightly associated with soil moisture decreases and act to offset water savings from reductions in stomatal conductance in response to high [CO_2]. Collectively our results connect the nonlinearity in carbon feedbacks to consequences for vegetation, hydrology, and future water availability in a high-[CO_2] world.

a. Greening and drying in the CMIP6

The CMIP6 ensemble mean COU simulation shows a consistent spatial pattern of vegetation "greening" and land surface "drying" implying healthy vegetation in the face of general reductions in water availability (**Fig. 1**). While the response is consistent with earlier model generations (Mankin et al. 2017a, 2018, 2019), its magnitude appears stronger in the CMIP6. The most salient indicator of this resides with GPP, which is the rate of plant photosynthesis (**Fig. 1a, S1**). The fully coupled ensemble mean COU response is to increase WY GPP by 68% over global land. The response is reflective of the productivity benefits of additional [CO_2] and the strengthening of the land carbon sink (**Fig. 1a, S1**). Complementing these productivity gains is additional carbon allocation to the leaves of plants, as measured by LAI, which increases by over 53% in the global mean (**Fig. 1b, S2**). The ensemble-mean responses in these two quantities, GPP and LAI, share consistent increases with each model in the COU run, though nuances in the spatial patterns vary (**Fig. S1, S2**). Notably, there is a 57% increase in canopy WUE, suggesting that plants are also more efficient in their water consumption (**Fig. 1c**). While the ubiquitous signal of the biogeochemical and physiological effects of [CO_2] on plants are clearly denoted by the widespread greening in **Figures 1a-c**, the shared water responses are far more heterogenous. A considerable fraction of land area, for example, has statistically significant WY drying in 1-m and 2-m soil moisture, as well as a reduction in WY total runoff (the sum of surface and subsurface runoff in the models). For example, approximately 50% of land areas have GPP and/or LAI increases collocated with 1-

and 2-m soil moisture declines and about 40% have runoff declines and such greening (**Fig. 1d-f**). These results suggest that for many locations, plant growth is unimpeded by regional land water reductions.

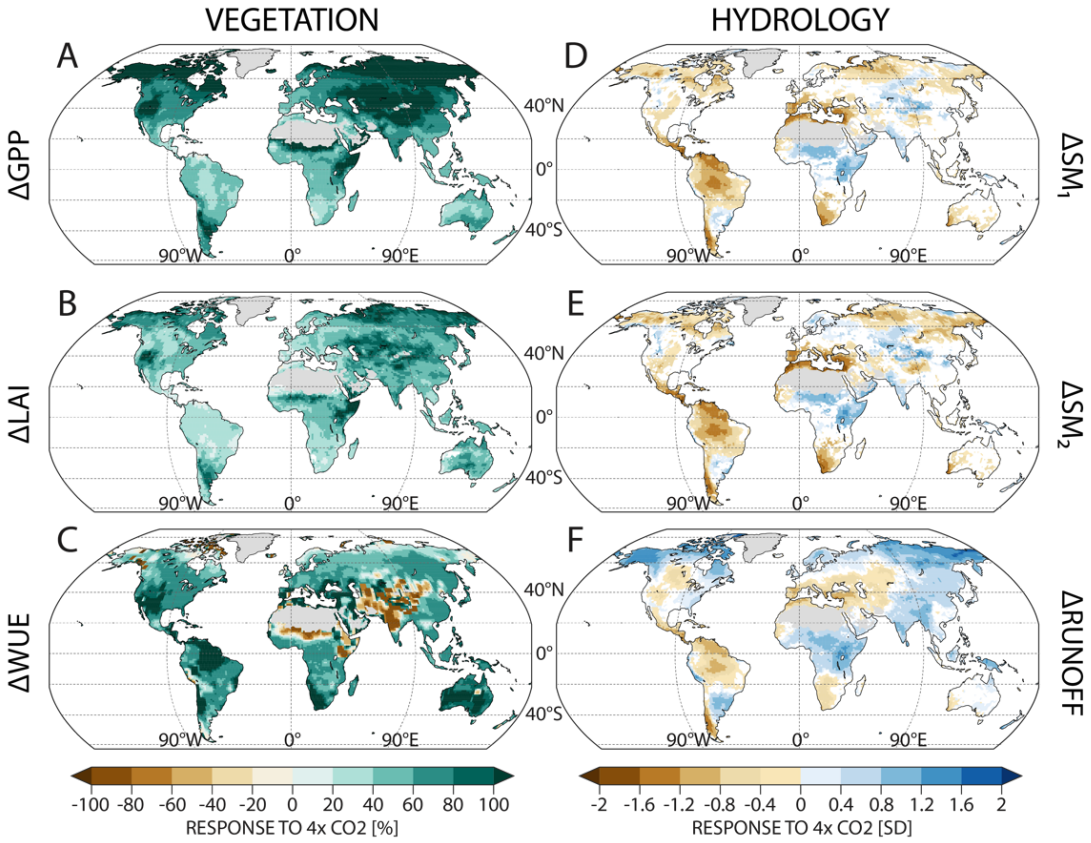

Fig. 1 Plant greening (in percent change, %) and soil drying (in standard deviations of change, SD) in the ensemble mean of the 1pctCO2 coupled simulation (COU). In response to 4xCO2 (taken as the climatological difference between the last and first 30 WYs of the simulations, **Section 2**), we show spatial patterns of changes in gross primary productivity, GPP (**a**), leaf area index, LAI (**b**), and ecosystem water use efficiency, WUE, calculated as the ratio of GPP to transpiration (**c**), all in percentage (%) changes. We also show the change in 1-m soil moisture (SM_1) (**d**), 2-m soil moisture (SM_2) (**e**), and total runoff (**f**), all in standard deviation (SD) changes. Only statistically significant changes are shown (**Section 2**).

b. Plant-relevant responses to high [CO_2] in the C4MIP experiments

Part of the power of the experimental design of the C4MIP is that it allows us to assess why the biogeochemical and radiative responses of plants to enhanced [CO_2] can result in vegetation greening and hydrological drying in the same grid points in the fully coupled COU simulations (**Fig. 1**). To illustrate this, we examine the ensemble and global mean responses of the physiological and radiative effects of increasing [CO_2] on terrestrial vegetation across

the three experiments, COU, BGC, and RAD (**Fig. 2**). As noted in **Section 2a**, comparing the BGC and RAD runs (one simulation in which plants are responsive to increasing [CO_2] and one in which they are not) to a third, fully coupled run (COU) in which all parts of the model respond to enhanced [CO_2], allows changes in plant water use and water availability to be attributed to radiative (e.g., warming) versus biogeochemical (e.g., plant physiological) effects.

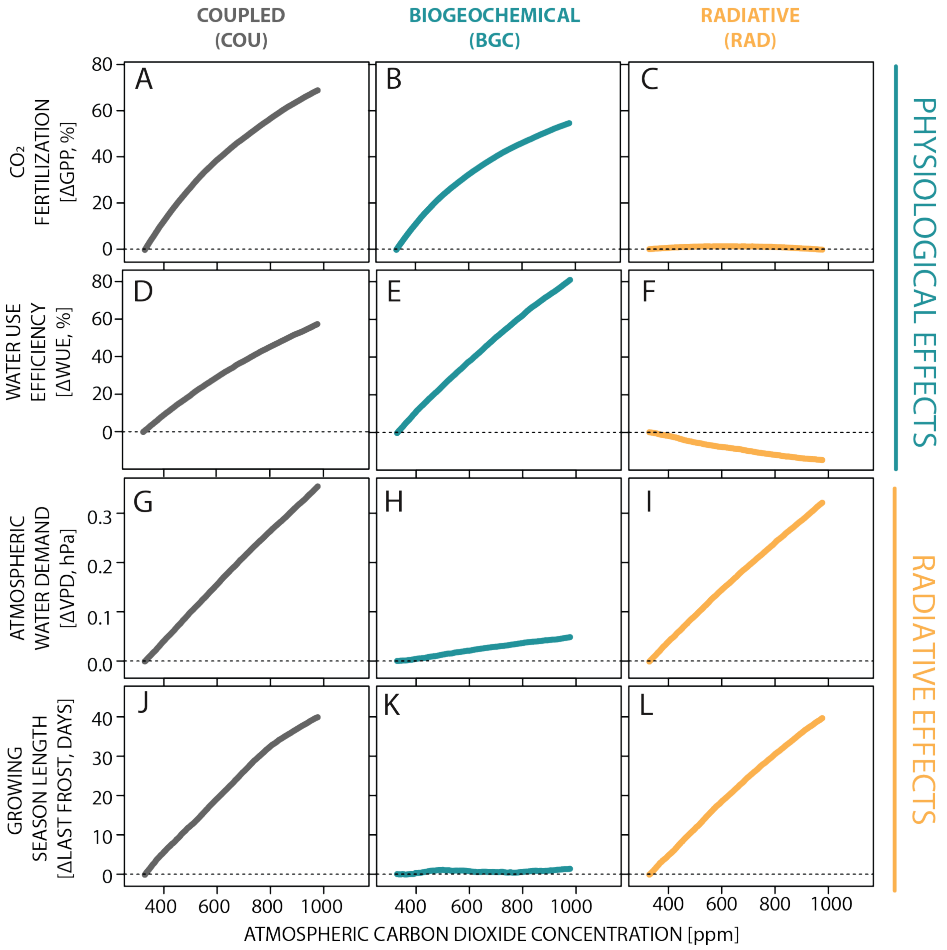

Fig. 2 Ensemble mean plant-related changes in response to the biogeochemical and radiative effects of enhanced CO_2 concentrations (in parts per million, ppm). For each of the fully-coupled experiment (COU), that where the biogeochemical response is isolated (BGC), or that where radiative response is isolated (RAD), we show the ensemble-mean global-land fertilization effect, estimated from gross primary productivity (GPP, %, **a.-c**.), water use efficiency (WUE, %, **d.-f.**), atmospheric water demand, proxied by the vapor pressure deficit (VPD, hPa, **g.-i**), and the growing season length, proxied by the advance in days of the last frost (**j.-l**.).

The CO_2-fertilization effect, as proxied by GPP, prevails in the COU run (**Fig. 2a**) due to the strong BGC response (**Fig. 2b**), with no contributions from RAD effects (**Fig. 2c**). Such enhanced GPP should tend to increase ecosystem water consumption and dry out the land. Stomatal closure under high [CO_2] yields increased WUE (**Fig. 2d**) and is considered to be the

dominant factor contributing to enhanced water availability under anthropogenic forcing, particularly when compared to radiative effects alone. In contrast, atmospheric water demand, as reflected in VPD (**Fig. 2g**), is driven predominantly by radiative effects (**Fig. 2i**). Plant water consumption would also be impacted by changes to the growing season length, which increases with forcing due to radiative, rather than biogeochemical, effects (**Fig. 2m-o**).

c. Nonlinear interactions between warming and [CO_2] enhance vegetation growth in CMIP6

Resolving the countervailing physiological and radiative responses presented in **Figure 2** is critical for appraising whether plants have a net wetting or drying effect under the full effects of CO_2 forcing. Such an effort, however, is complicated by the potential for nonlinear interactions among the radiative and biogeochemical effects of CO_2. Prior work using earlier generations of C4MIP have assumed that the BGC and RAD effects can be linearly decomposed, including investigations of how plant responses impact water availability under high-[CO_2] (Swann et al. 2016; Fowler et al. 2019; Arora et al. 2020; Zhou et al. 2023); however, the assumption of linearity in carbon feedbacks does not hold in CMIP6 (Huang et al. 2022).

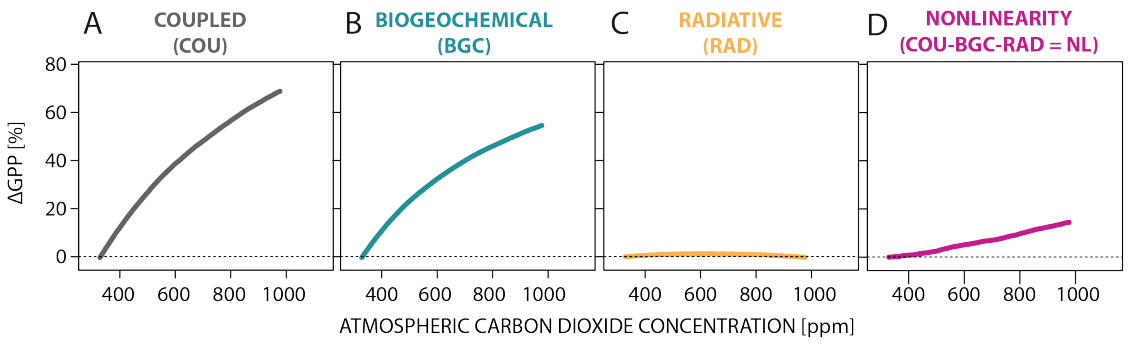

Fig. 3 An emergent nonlinear term in vegetation productivity in the C4MIP **a-d,** The ensemble mean percent change in gross primary productivity (ΔGPP, %) in each of the three experiments, the coupled (COU, **a**), the biogeochemical (BGC, **b**), the radiative (RAD, **c**), and the nonlinear term (NL, **d**) that is calculated as the experimental residual all presented as a function of increasing [CO_2].

In analyzing the linearity assumption for the CMIP6 C4MIP experiments, there is a large and significant nonlinear response of enhanced plant growth from the interaction of radiative and biogeochemical effects of high [CO_2] (**Fig. 3**). This response can be seen in **Figure 3d**, where a nonlinear term in GPP, which we term GPP_{NL}, increases by ~35% beyond that predicted by the biogeochemical or radiative effects, or their sum, alone. The magnitude of this nonlinear

GPP term is sizable—it is equivalent to ~25% of the fully coupled COU response in GPP at a quadrupling of [CO_2].

While such an interaction between [CO_2] and warming is expected in the real world, sizable interactions between RAD and BGC across the ESM ensemble is a new feature in CMIP6. We can compare the nonlinear plant terms calculated with CMIP6 versus that from an earlier generation, CMIP5. Nonlinear interactions between the radiative and biogeochemical effects of high [CO_2] on carbon and plants were smaller and less uncertain in CMIP5 than in CMIP6 (**Fig. 4**). Consider for example, the change across generations in GPP_{NL} (**Fig. 4a**). Two features are worth noting here. First is the expected and tight association between ensemble variation in GPP_{NL} and LAI_{NL} across both ensembles—positive nonlinear GPP changes imply positive nonlinear leaf area growth. Second, however, is that the strength of this relationship and the inter-model variation in the magnitude of these nonlinear terms is considerably larger in CMIP6 than in CMIP5. The ensemble spread in GPP_{NL} in the CMIP5 spans ±10%, approximately half the range found in CMIP6 (**Fig. 4a**). Moreover, the CMIP5 ensemble range in LAI_{NL} is less than a third of that for CMIP6 (e.g., compare relative spans of the bars mapped to the y-axis in **Fig. 4a,b**).

The larger uncertainty and magnitude of carbon interactions across model generations suggests that the assumption that carbon feedbacks can be linearly decomposed into those arising from biogeochemistry or radiative effects alone, or that any carbon feedback nonlinearity is trivial does not hold for CMIP6 (**Figs. 3 and 4**). The large nonlinear terms in GPP presented in **Figure 3** are invariably tied to the carbon cycle and are critical to understand, particularly given the ongoing efforts to constrain model uncertainty in land carbon responses to forcing (Hall et al. 2019; Liu et al. 2023; Wenzel et al. 2014). While GPP, NPP, and NEE are all tightly related quantities, here we show the strength of their nonlinear terms are also positively correlated across the ensemble: changes in NEE_{NL} are directly related to the changes in GPP_{NL} across the ensemble (**Fig. 4b**). NEE_{NL} is very tightly correlated with that from GPP_{NL} across both the CMIP5 and CMIP6 ensembles, with a strong positive relationship consistent across model generations. There is, however, a far larger range of modeled NEE_{NL} values in the CMIP6 than in the CMIP5, suggesting a growing uncertainty in carbon interactions across generations.

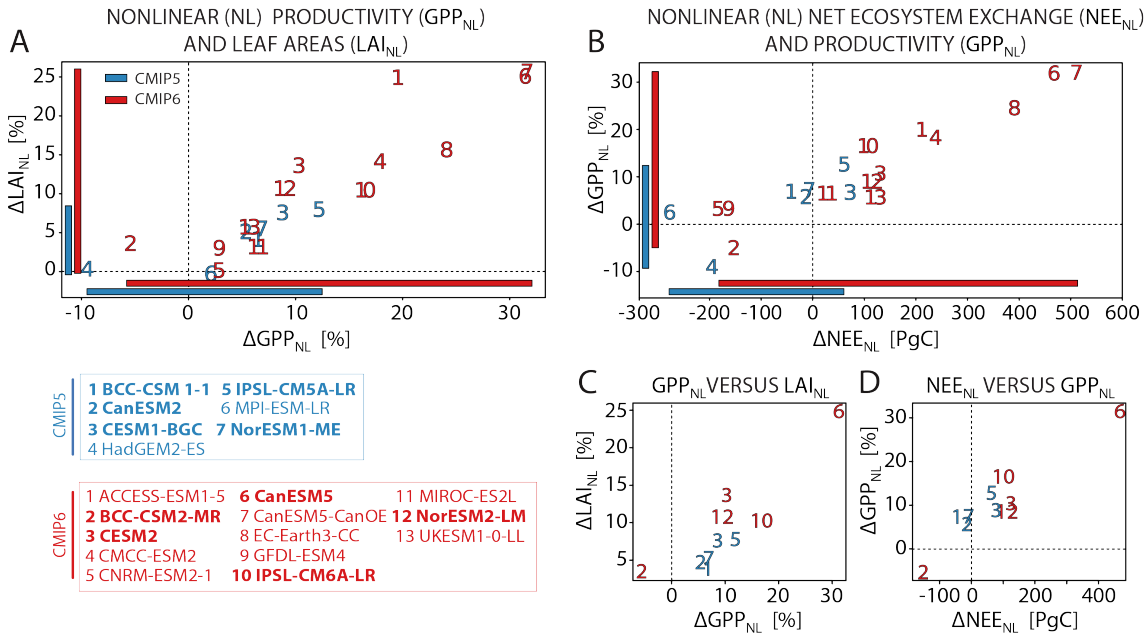

Fig. 4 The inter-model association between nonlinear vegetation terms in CMIP5 and CMIP6. We show the variation in (**a**) GPP_{NL} and LAI_{NL} and (**b**) in NEE_{NL} and GPP_{NL} in CMIP5 (blue) and CMIP6 (red) for all vegetated land areas. The full model range is mapped to each axis via the colored bars. Panels (**c**) and (**d**) show the same set of results as in (**a**) and (**b**) but for the subset of models that are available for both generations of CMIP (bolded models in legend): BCC-CSM 1-1 and BCC-CSM2-MR; CESM1-BGC and CESM2; CanESM2 and CanESM5; IPSL-CM5A-LR and IPSL-CM6A-LR; NorESM1-ME and NorESM2-LM. It is clear that the CMIP6 spans nearly double the range of that from the earlier CMIP5, suggesting a growth in uncertainty due to nonlinear interactions among biogeochemistry and warming across generations.

The growth in RAD-BGC interactions in CMIP6 relative to CMIP5 is perhaps related to the increased complexity of terrestrial biogeochemical processes across model generations. Future work should focus on identifying the processes that contribute the most to the magnitude of the nonlinear RAD-BGC interactions. Hypotheses to test could include whether the representation of nutrient cycles, or other processes, such as ecosystem disturbance, succession, and mortality account for the change from CMIP5 to CMIP6. It is certainly the case that more models are representing nitrogen and phosphorous cycles and vegetation cohort dynamics (Fisher and Koven 2020). As such, a rigorous model-by-model investigation of which key model choices have shaped the growing interactions between RAD and BGC changes is essential to better-constrain the land carbon sink under warming and its consequences for water and warming.

At the same time, while increased model complexity is a possible contributing factor, an expanding range in these nonlinearities could simply be a function of the larger number of

participating models in CMIP6 or the increase in modeling centers contributing simulations. To assess whether the growing CMIP uncertainty is robust, we consider the subset of five models that have the requisite data available across both generations (**Fig. 4c,d**). The results show that even when considering paired models across generations and the same number of models, CMIP6 spans a far greater range of nonlinear carbon flux values than CMIP5. All five models except those from the Beijing Climate Center (BCC models) show an increase in in LAI_{NL}, GPP_{NL}, and NEE_{NL}—some as large as 20 percentage points—as is the case for the Norwegian model (NorESM). These results suggest that the magnitude of nonlinear uncertainties has expanded in the CMIP6 relative to the CMIP5.

d. Nonlinear vegetation growth in CMIP6 tied to carbon feedback parameters

The large nonlinear vegetation response to enhanced [CO_2] present in CMIP6 models (Huang et al. 2022) raises questions about their implications for carbon feedbacks and land hydrology. To provide some insights into the former, we extend earlier analyses (e.g., Huang et al. (2022)) and examine two key carbon feedback metrics estimated from the C4MIP simulations, as detailed in the Section 2 (Arora et al. 2020; Jones et al. 2016): the carbon-concentration feedback, β, and the climate-carbon feedback, ɣ. Positive values of β or ɣ indicate land carbon gains in response to increasing [CO_2] and temperature (**Fig. 5**).

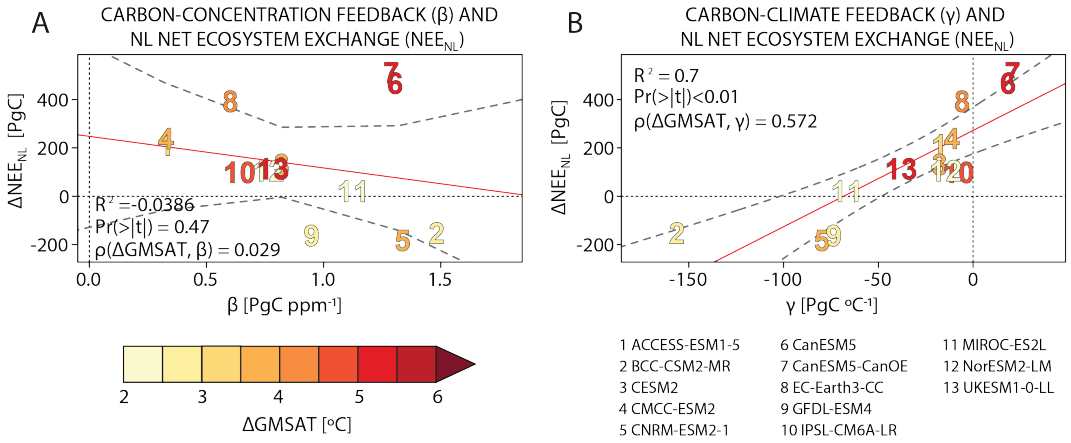

Fig. 5 Nonlinear carbon feedbacks and their association with vegetation growth for global land areas in CMIP6. **a,** The ensemble association between the nonlinear term in net ecosystem exchange (NEE_{NL}) and the carbon-concentration feedback, β. **b,** The inter-model association between the nonlinear term in net ecosystem exchange (NEE_{NL}) and the carbon-climate feedback, ɣ. Colors indicate the magnitude of each COU model's 2-m global mean 4xCO2 surface air temperature (GMSAT) 4xCO2 response (land and ocean). The 13 models included in the analysis are listed. Inset text in each panel indicates the R-squared derived from a linear regression, shown as a red line, the significance of that regression, and the correlation between the x- and z-axis variables. Dotted grey lines indicate the 95% prediction-based confidence interval.

We find that carbon nonlinearities (exemplified by NEE_{NL}) scale much more tightly with model variation in the land-carbon sensitivity to climate (ɣ, **Fig. 5b**), than to higher [CO_2] concentrations (β, **Fig. 5a**). In particular, models in which GPP is amplified by the interactions of warming and [CO_2] have larger values of GPP_{NL}, larger values of LAI_{NL}, and they also stimulate stronger carbon uptake than release by heterotrophic respiration (a positive NEE_{NL}) relative to models with weaker nonlinear terms (**Fig. 4**). These same models also tend to be warmer than models with weaker nonlinearities, denoted by the global mean surface air temperature (GMSAT) changes from the COU in **Figure 5**. As a consequence, the models with strong nonlinearities in carbon exchange tend to have less negative or even positive values of ɣ (**Figs. 5b**). Weaker carbon-climate feedbacks (ɣ) imply either stronger carbon assimilation by the land, less land carbon lost from warming-induced heterotrophic respiration, or some combination thereof, making for a more resilient land-carbon sink under climate change (**Fig. 5b**). In contrast, models with smaller GPP_{NL} have less amplified LAI_{NL} (**Fig. 4a**), weaker or negative NEE_{NL} (**Fig. 4b**), less warming (**Fig. 5**) and a more negative ɣ (from the land perspective), indicating larger land carbon losses to the atmosphere per degree of warming (**Fig. 5b**).

Decomposing NEE into its components, net primary productivity (NPP) and heterotrophic respiration (RH), confirms the above interpretation and further emphasizes that these nonlinear carbon terms are more tightly associated with ɣ than with β (**Fig. 6**). Cumulative changes in NPP and RH from the COU run, for example, tightly scale with β, rather than with ɣ, (cf. **Fig. 6a,e and c,g**). Such an association is expected and intuitive: β is dominant in shaping the total carbon cycle response to climate change in the fully coupled models (Arora et al. 2020). What is notable, however, is that this pattern reverses entirely when considering nonlinear terms, such as NPP_{NL} and RH_{NL} (cf. **Fig. 6b,f and d,h**). Across the CMIP6 ensemble, the magnitude of ɣ tightly corresponds with the magnitude of the RAD-BGC interactions terms in net primary productivity, NPP_{NL}, and respiration, RH_{NL}

(**Fig. 6f,h**). Both of those terms also shares a tight positive association with NEE_{NL} and GPP_{NL} (**Fig. 6i-l**).

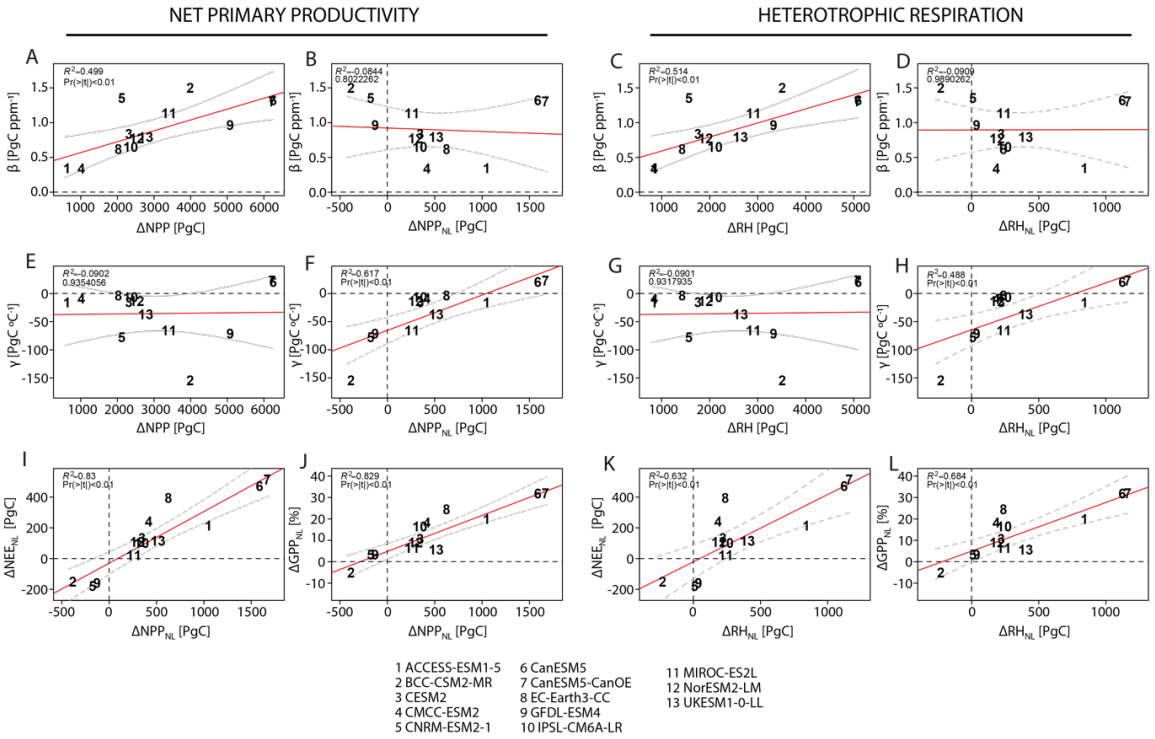

Fig. 6 The CMIP6 inter-model association between the components of NEE, NEE_{NL} and carbon feedback metrics for global land areas. We show cumulative changes in net primary productivity, cumulative NPP and cumulative NPP_{NL}, left side, and heterotrophic respiration, RH and RH_{NL}, right side, all in of petagrams of carbon (PgC) and carbon feedbacks, β (**a-d**) and ɣ (**e-h**) for each model. We also show the model-by-model association between NEE_{NL} and GPP_{NL} and the components that comprise each term (**i-l**). Ensemble variation in NPP and RH changes from the COU are tightly associated with β (**a, c**) (as opposed to ɣ (**e, g**)). However, the nonlinear components NPP_{NL} and RH_{NL} are not associated with β (**b, d**). Instead, these nonlinear terms are tightly associated with variation in ɣ (**f, h**), and are closely related to NEE_{NL} and GPP_{NL} (**i-l**). R-squared values and the significance of each regression is shown in the top left of each panel.

e. Nonlinear interactions between warming and [CO_2] enhance plant-based ET

To examine how the nonlinear terms in vegetation growth influence ecosystem water use, we use a simple hydrologic budget following earlier work (Mankin et al. 2019, 2018). We analyze changes in how WY precipitation (P) is partitioned at the land surface among three terms: the canopy water flux (C), total runoff (Q), and soils (S) (see **Section 2**). To illustrate that this budget is reasonable and that there is, in fact, closure among the terms, we plot the ensemble mean percentage of total WY precipitation going to each term—C, Q, and S—in the first 30 years of the COU run (**Fig. 7**). If there is closure, then the sum of the partitioning ratios C/P, Q/P, and S/P should approach 100%. We find they do for most

528 regions, save for a small portion of High Mountain Asia (**Fig. 7d**), where multiyear snowpack
529 (**Section 2**) is present in both observations and models (Gottlieb and Mankin 2024).

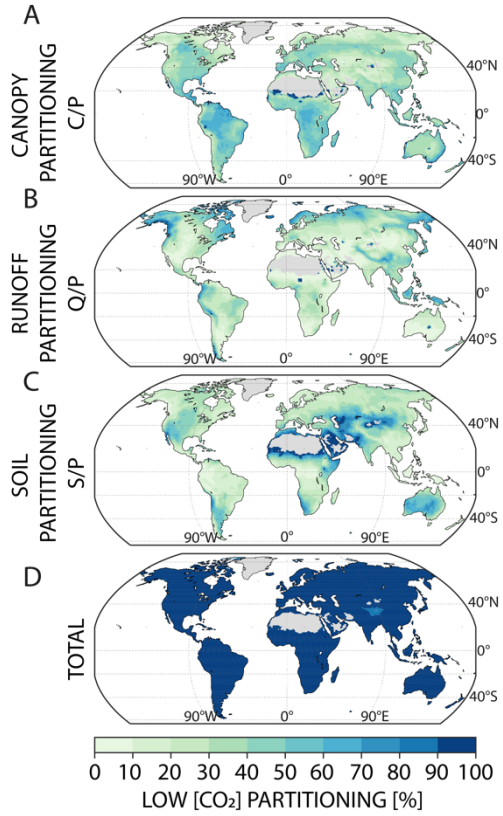

530

531 **Fig. 7** Ensemble mean precipitation partitioning during the first 30 years of the 1pctCO2 (COU) simulation
532 expressed as a percent (rather than fraction) for the canopy (C/P) (**a**), runoff (Q/P), (**a**), and soils (S/P), (**c**).
533 The sum of the three ratios (**d**) should approach 100% assuming that at climatological WY scales as
534 P=C+Q+S.

535

536 Maps of total changes in WY hydrologic variables (**Fig. 8**) and their relative changes
537 from precipitation partitioning (**Fig. 9**) show that nonlinear terms increase plant-based ET
538 both relatively (as a fraction of precipitation) and absolutely (in standard deviations of
539 change) in response to high [CO_2]. As expected, and consistent with the pattern of the fully
540 coupled ensemble mean response to forcing, precipitation in the COU increases in the
541 extratropical northern latitudes and equatorial Africa and Asia, with drying in the
542 Mediterranean, the Amazon, Central America, southern Africa and Chile, and uncertain
543 change elsewhere (**Fig. 8a**). Across most of the budget terms, P (**Fig. 8a-d**), C (**Fig. 8e-h**), Q
544 (**Fig. 8i-l**), and S (**Fig. 8m-p**), the ensemble mean pattern in the COU is primarily driven by
545 the forced climate response in the RAD, more so than the BGC or NL terms, which are
546 modest in the ensemble mean, if and where they are significant. This response is because P

changes are driven by the thermodynamic response in the RAD, whereas forced P responses in the BGC are smaller (though still potentially important) (Skinner et al. 2017; Lesk et al. 2025).

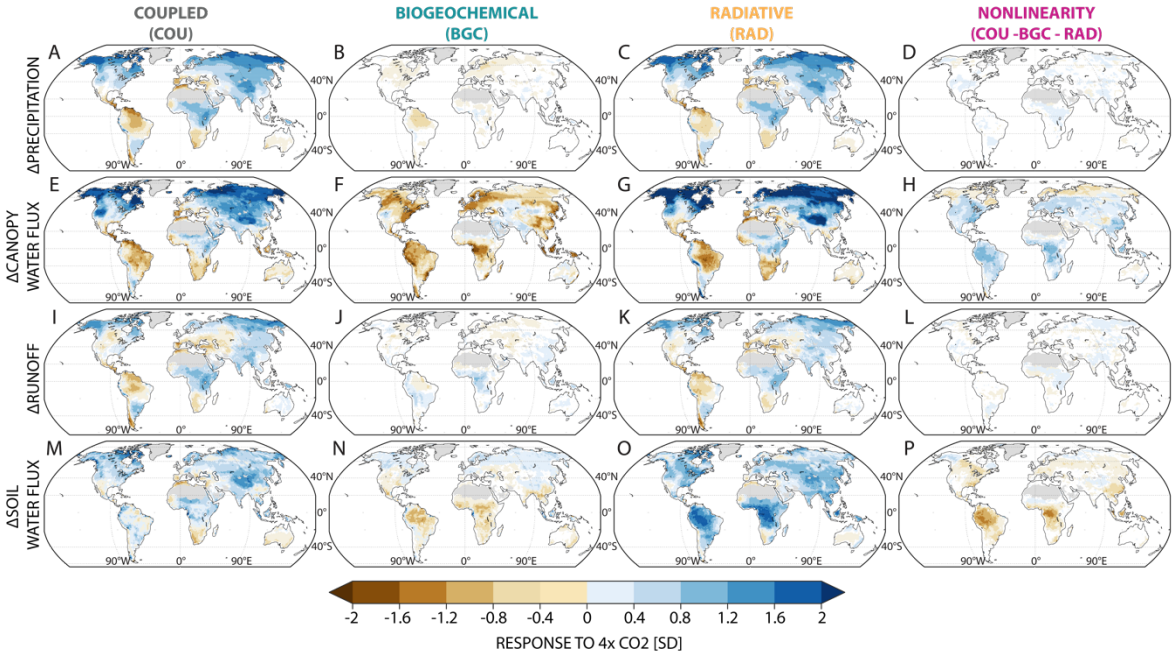

Fig. 8 Hydrologic changes across experiments under the water budget of P = C + Q + S, presented in standard deviations of change (SD) in response to 4xCO2. The ensemble mean response of precipitation (**a-d**), canopy water flux, C (**e-h**) total runoff (Q, **i-l**), and soils (change in 2-m soil moisture storage plus soil evaporation, **Section 2**, **m-p**) in the fully coupled experiment (COU), the experiments in which the biogeochemical response is isolated (BGC), the radiative response is isolated (RAD), and the residual or nonlinear interaction between the RAD and BGC (calculated as COU-BGC-RAD). Gray regions indicate where historical peak leaf area index is below 0.1. Only statistically significant changes (K-S test, $p<0.05$) are shown and all maps are at the WY scale.

Beyond the pattern of precipitation changes, the stomatal response from higher [CO_2] in the BGC run clearly leads to a global-scale reduction in plant-based ET, the C term in our budget (**Fig. 8f**). The ubiquity of the brown contours in **Figure 8f** is striking, and it is this response in the C4MIP BGC that gives rise to the suggestion that plant physiological responses to enhanced [CO_2] will tend to enhance water availability for soils or rivers, offsetting the drying from RAD effects or CO_2 fertilization. However, the NL term for plant-based ET, C_{NL} (**Fig. 8h**), shows a pattern of *increases* that roughly mirrors the *reductions* in plant-based ET in the BGC run (**Fig. 8f**). This means that nonlinear interactions between the radiative and biogeochemical effects cancel any plant-water savings from the BGC run,

leaving the RAD run to dominate the COU pattern. It is also noteworthy that there are decreases in the S_{NL} term (**Fig. 8p**), which we explore further in later sections.

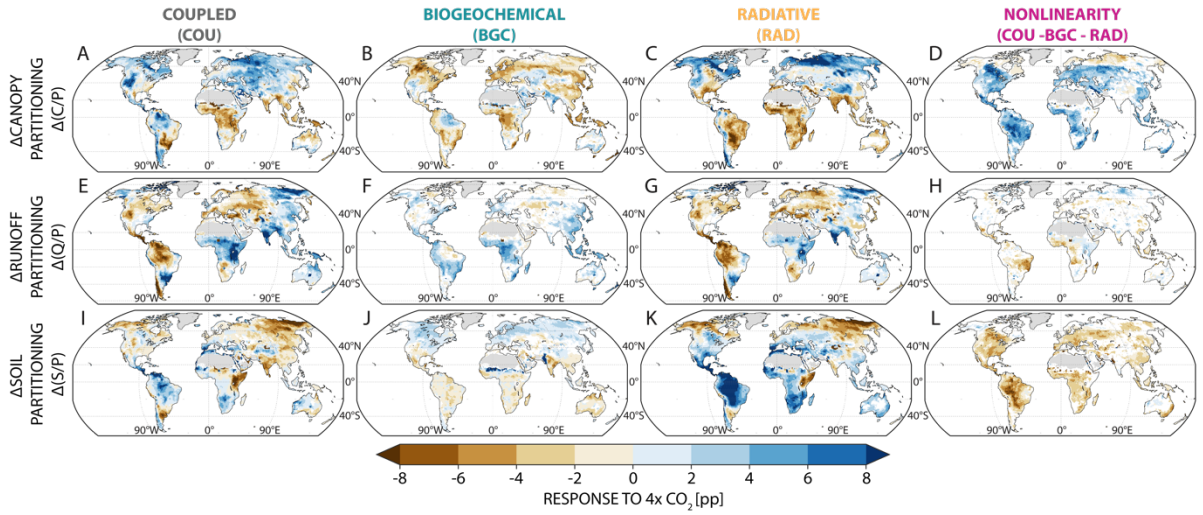

Fig. 9 Changes in WY precipitation partitioning at the land surface to each term in the hydrologic budget in response to 4xCO2, presented in percentage points (pp) of change. For each experiment and the NL term (columns) we show the spatial pattern of changes in the fraction of total WY precipitation directed to canopies, Δ(C/P) (**a-d**), runoff, Δ(Q/P) (**e-h**), and soils, Δ(S/P) (**i-l**) (see **Section 2**). Gray regions indicate where historical peak leaf area index is below 0.1. Only statistically significant epoch changes (K-S test, $p<0.05$) are shown.

The nonlinear terms are robust in the parts of land hydrology most closely associated with vegetation; this pattern also persists when we examine relative changes in precipitation partitioning. The maps in **Figure 9** show the change in the fraction of WY precipitation allocated to each hydrologic budget term, C, Q, and S. In the fully coupled COU run, the change in canopy partitioning, Δ(C/P), increases across vast swaths of the globe, particularly in the northern and eastern hemispheres (**Fig. 9a**) as plants in those regions demand larger fractions of each drop of precipitation. In tropical Africa and Asia, canopy partitioning declines (**Fig. 9a**), likely due to WUE and stomatal closure effects being stronger than CO_2 fertilization in the BGC runs (**Fig. 9b**) and because of either reduced precipitation or higher VPD in the RAD runs (**Fig. 9c**). Fully coupled changes in runoff partitioning, Δ(Q/P), show declines over much of the northern and eastern hemispheres (**Fig. 9e**), driven predominantly by radiative warming (**Fig. 9g**), and show increases in tropical Africa and Asia through contributions from both the biogeochemical and radiative effects of increasing [CO_2]. The BGC contribution to increased Q/P and decreased C/P (cf. **Fig. 8f, j and Fig. 9b, f**) is the "plants turn on the tap" response (Jasechko 2018), where stomatal closure and WUE

increases spare water for runoff and or soils. Lastly, there are the changes in soil partitioning, Δ(S/P) (**Fig. 9i-k**), which outside of western North America, shows an inverse pattern to runoff partitioning in the COU run (cf. **Fig. 9e, i**) driven largely by radiative effects (**Fig. 9k**). Because the partitioning ratios sum to unity (**Fig. 7**), changes are bounded such that increases in one term must be compensated by decreases in another.

Importantly, changes in precipitation partitioning at the land surface for the COU run do not equal the sum of changes in the BGC and RAD components. A large, positive, and statistically significant $(C/P)_{NL}$ spans most regions globally in the C4MIP (**Fig. 9d**), a feature that is associated with decreased $(Q/P)_{NL}$ and, primarily, $(S/P)_{NL}$ (**Fig. 9h and l**). Increases in $\Delta(C/P)_{NL}$ shown in **Figure 9d** arise from some combination of changes in transpiration and leaf evaporation, which are combined in the C term.

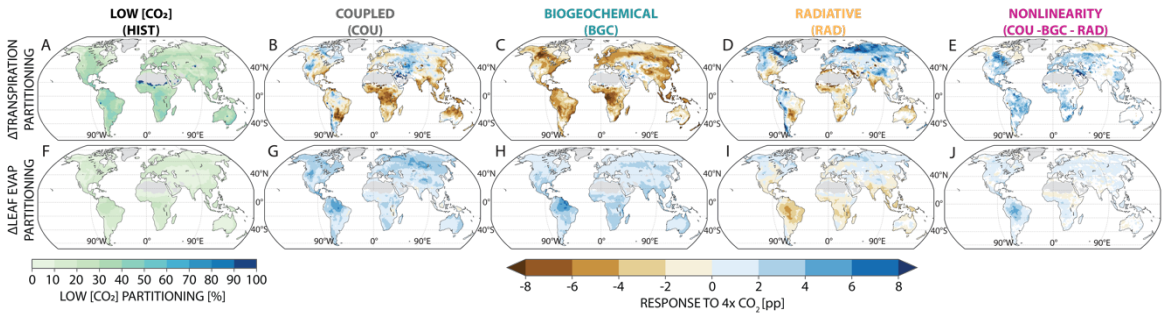

Fig. 10 WY precipitation partitioning and its changes across experiments to the components of plant-based ET in percentage points of change (pp). The ensemble mean low [CO_2] partitioning, defined as the first 30 years of the 1pctCO2 (COU) run (first column, **a,f**) and then its change in the COU (second column, **b,g**), BGC (third column, **c,h**), RAD (fourth column, **d,i**) simulations, and then in the NL term (fifth column, **e,j**). We show the response for transpiration partitioning (first row **b-e**, calculated as WY changes, Δ(TRAN/P)) and leaf evaporation partitioning (second row, **g-j**, calculated as $\Delta(E_L/P)$).

We decompose canopy partitioning (the C term) into its components, transpiration and leaf evaporation, in **Figure 10**. It is clear that positive $(C/P)_{NL}$ changes are driven by a nonlinear term in transpiration partitioning, though important contributions also come from increased leaf evaporation (**Fig. 10e, j**). In other words, while BGC responses alone are associated with plant responses that diminish transpiration and thus spare water for runoff and soil moisture (cf. **Fig. 9b, f, j**), that alone does not shape plant-based ET changes. Nonlinear interactions between BGC and RAD responses favor relative increases in plant-based ET to the sacrifice of runoff and soil moisture when controlling for precipitation changes (cf. **Fig. 9d,h,l)**, predominantly by enhancing transpiration (**Fig. 10e**) even in the face of stomatal closure. The consequence of RAD and BGC interactions is an increase in

plant-based ET relatively and absolutely, reducing soil water (**Figs. 8p and 9l**), and to a lesser extent, runoff partitioning (**Fig. 9h**).

It is notable that this nonlinear increase in relative plant water use is insensitive to the sign of precipitation change (**Fig. 11**). To make this assessment, we divide global grid points into regions where precipitation increases versus where it decreases based on COU 4xCO2 response (**Fig. 11a,b, Section 2**). For each of these domains, we present the area-weighted average response as a function of [CO_2] in each experiment as well as the NL term (**Fig. 11c-h**). Regardless of the precipitation change, there is a significant increase in precipitation that is partitioned to plants from the nonlinear interactions between the radiative and biogeochemical effects of [CO_2] (**Fig. 11c,d,** bolded pink lines). It is also interesting that in regions with decreased precipitation, there is a significant decrease in runoff partitioning from the NL term that emerges under high [CO_2], countering any increase in runoff partitioning from the BGC (cf. the pink and green lines in **Fig. 11f**). There is essentially no statistically significant enhancement of runoff partitioning in precipitation positive regions, suggesting that mean precipitation changes alone do not account for runoff enhancement (**Fig. 11e**). Notably, we find that increases in extreme precipitation are more tightly associated with increasing runoff partitioning than mean precipitation (**Fig. S4**).

Regardless of the precipitation change, the NL term acts to decrease precipitation partitioning to soils, denoted by the statistically significantly declines (**Fig. 11g,h,** pink lines). The direction of precipitation change appears to affect the extent to which runoff partitioning or soil partitioning is affected, with precipitation decreases leading to an increase in $(C/P)_{NL}$ (pink line in **Fig. 11d**), and a decrease in $(Q/P)_{NL}$ and soils $(S/P)_{NL}$ (pink lines in **Fig. 11f**, and **h**, respectively). Together, these results indicate that the NL increase in plant-based ET occurs regardless of the sign of precipitation change and can diminish water partitioning to soils and runoff. This response occurs in spite of enhanced WUE and surface resistance to ET that are thought to be key to runoff enhancement or drought-risk reductions (Roderick et al. 2015; Swann et al. 2016; Fowler et al. 2019). Where canopy partitioning does decrease, such as from the BGC effect (statistically insignificant segments of green lines in **Fig. 11c,d**), the nonlinear term acts to weaken or completely counter that effect (statistically significant segments of pink lines in **Fig. 11c,d**).

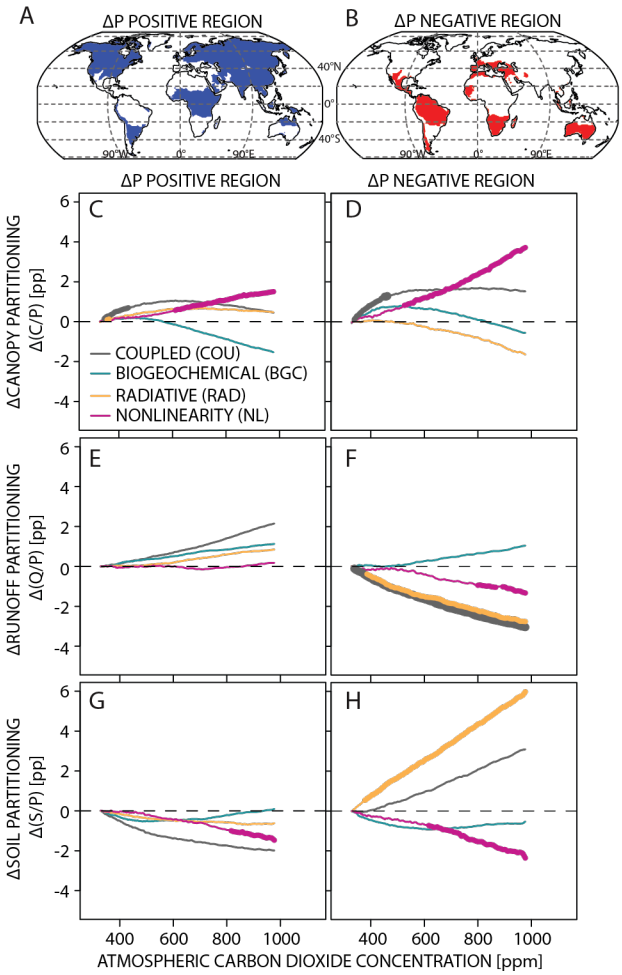

Fig. 11 Precipitation partitioning responses in percentage point change (pp) to increasing [CO_2] in ppm. Maps show the regions of ensemble mean precipitation increases in blue (**a**) and decreases in red (**b**) from the COU run. These maps define the domains over which we evaluate the ensemble mean changes in each experiment for each quantity presented in panels **c-h**. The ensemble mean area-weighted regional average responses in percentage points [pp] of canopy partitioning, C/P (**c-d**), runoff partitioning, Q/P (**e-f**), and soil partitioning S/P (**g-h**) in precipitation increasing (**a**) and decreasing (**b**) regions as a function of [CO_2]. Ensemble statistical significance is presented as a bolded line (**Section 2**).

The changes in precipitation partitioning due to nonlinear interactions between the RAD and BGC runs generate wide changes in land hydrology. To illustrate the connection between the relative changes presented in **Figures 9-11** and the changes presented in **Figure 8**, we divide global land areas into three regions, one in which ensemble mean COU 4xCO2 changes in canopy partitioning are positive (called "Δ(C/P) positive region"), one in which COU changes in runoff partitioning are positive (or "Δ(Q/P) positive region"), and one in which COU changes in soil partitioning are positive (or "Δ(S/P) positive region") (**Fig. 12a-c, S4**). We note two revealing patterns of hydrologic change: First, the precipitation increase in the Δ(Q/P) positive region is far larger than in the Δ(C/P) positive region, as precipitation

changes have a first-order control on enhancing runoff partitioning and total runoff, even in the BGC run (cf. **Fig. 12d and e** with **Fig. 12k and l**).

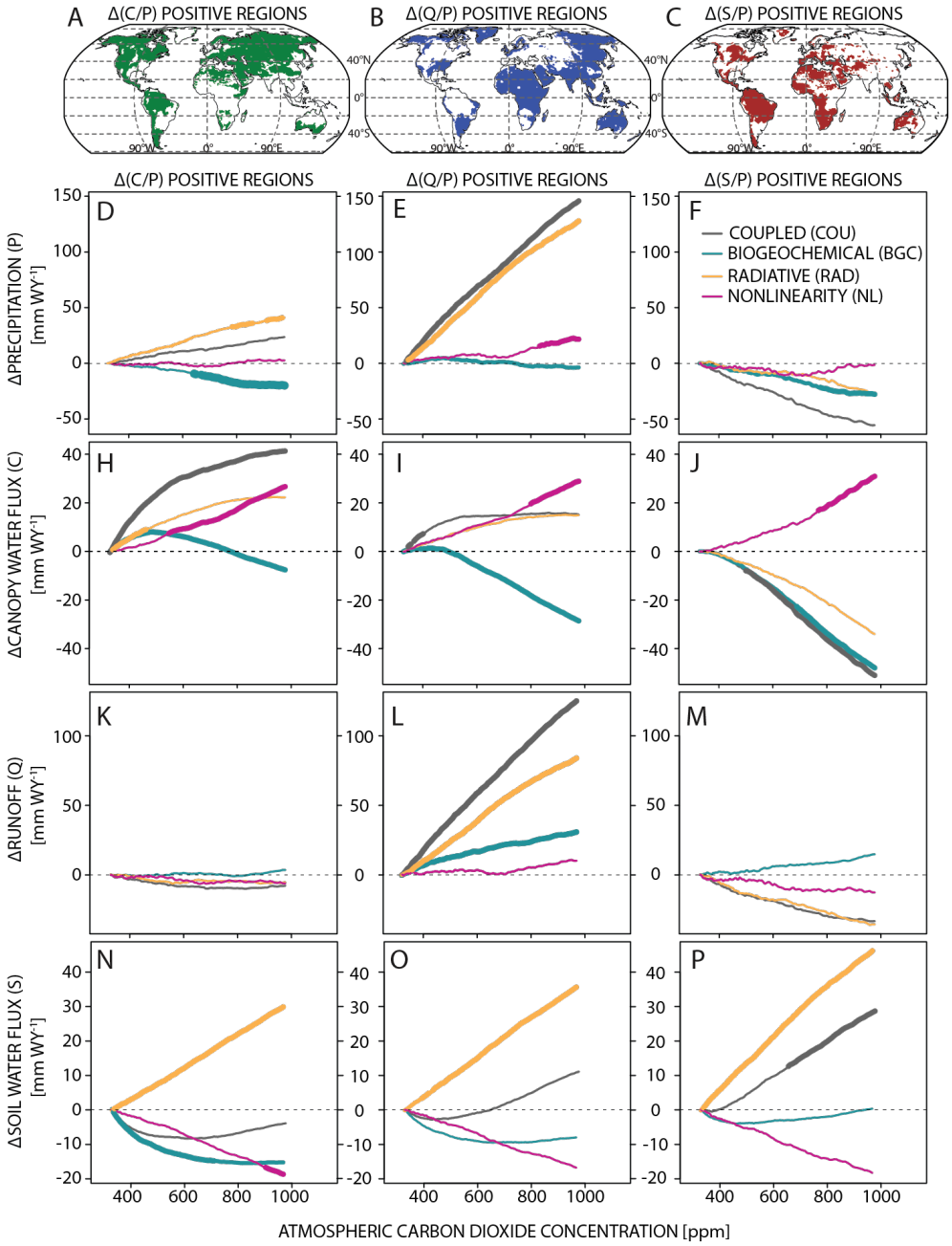

Fig. 12 Total hydrologic changes in mm per WY across experiments and the nonlinear terms in response to increasing [CO_2] in ppm. Maps (**a-c**) of regions where the ensemble mean partitioning increases for Δ(C/P), Δ(Q/P), and Δ(S/P), based on the COU 4xCO2 response (see maps in **Fig. 9, a, e, i**). The maps in (**a-c**) define the domains over which we evaluate the ensemble mean change in total hydrologic quantities in mm per WY presented in panels **d-p**, linking how the partitioning changes shape total changes in C, Q, and S. For each partitioning increase region, we show the time series of ensemble mean precipitation changes (**d-f**), canopy water flux, C, changes (**h-j**), runoff, Q, changes (**k-m**) and soil water, S, changes (**n-**

p) in each experiment and the nonlinear term. Ensemble statistical significance in the time series is presented as a bolded line.

The Δ(S/P) and Δ(C/P) positive regions contrast with the Δ(Q/P) positive regions in that they have no statistically significant change in precipitation in the COU run (**Figure 12d,f,** thin gray lines). Second, and consistent with the nonlinear term in carbon and in plant-based ET, our results also demonstrate a clear—and previously unaccounted for—significant nonlinear increase in the canopy water flux, C (and its components: transpiration and leaf evaporation), regardless of the partitioning region (bolded pink lines in **Fig. 12h-j**)**.** Such ubiquity suggests that the nonlinear term in canopy partitioning, or $\Delta(C/P)_{NL}$, is associated with a positive nonlinear term in the absolute plant-based ET (ΔC_{NL}) as well, regardless of whether canopy partitioning increases in the COU run. These changes are sizable, amounting to more than 50% of the canopy water flux response in the COU experiment. The widespread increase in plant-based ET from interactions between BGC and RAD runs cancel or exceed any water savings that accrue in the BGC runs from stomatal closure in the CMIP6 across precipitation changes (**Fig. 11**), or hydrologic partitioning changes (**Fig. 12**).

Nonlinear plant-based ET reduces soil moisture while runoff is controlled by precipitation

To connect our two sets of results—the nonlinear vegetation growth from carbon feedbacks (**Fig. 3-6**) and the nonlinear hydrologic changes (**Figs. 8-12**)—we examine inter-model global changes in C, Q, and S, as well as their grid-point responses to evaluate whether they are consist across model spatial scales and within individual models (**Fig. 13**).

At the global scale, and across all models in the C4MIP ensemble, the magnitude of C_{NL} is significantly and positively correlated with LAI_{NL}, accounting for over 50% of the inter-model variation in the C4MIP (**Fig. 13a**). Positive leaf-area nonlinearities (LAI_{NL}) are closely tied to nonlinear changes in GPP_{NL} (**Figs. 4-6**), suggesting the RAD-BGC interactions in carbon cycle processes amplify plant growth and consequent ET. We pool all model grid points together, bin them into their LAI_{NL} and C_{NL} responses, and calculate the average of $\Delta(C/P)_{NL}$ across all model grid points falling in each LAI_{NL} and C_{NL} bin (**Fig. 13b, Section 2**). While LAI_{NL} is positive in the ensemble mean everywhere, across the full model distribution, there are grid points within individual models with negative values (**Fig. 13b**). Across spatial scales there is a clear positive correlation between LAI_{NL} increases, C_{NL} increases, and $(C/P)_{NL}$ increases. The positive association among all three is strong,

713 suggesting that plant growth nonlinearities influence both the relative and absolute increases
714 in simulated ecosystem water use across models, regions, climates, and biomes.

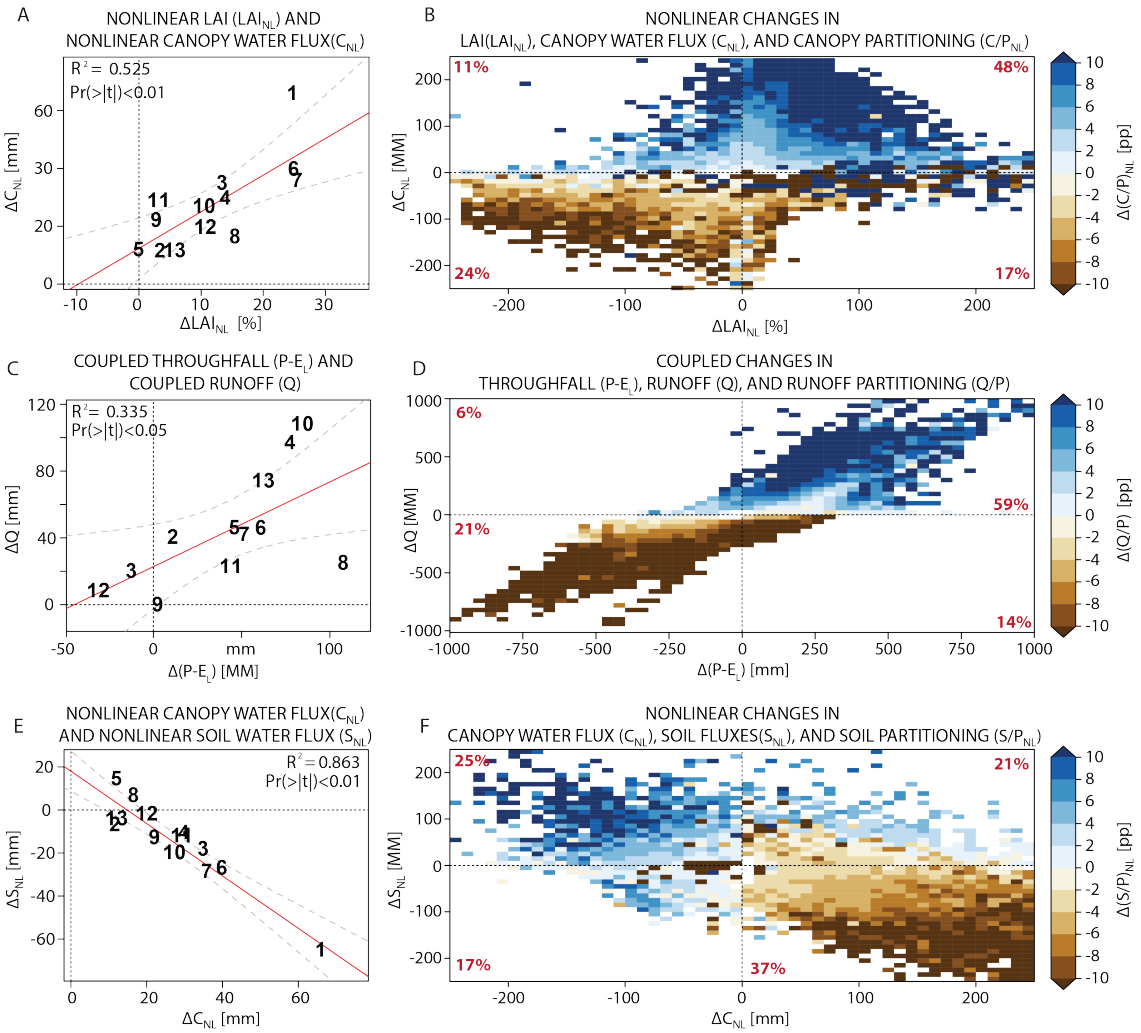

715

716 **Fig. 13** Linking plant greening to soil drying in the C4MIP. **a**, The inter-model association between the
717 4xCO2 response in the nonlinear LAI term (LAI_{NL}, %) and the nonlinear canopy water flux term (C_{NL}, mm
718 WY^{-1}) over global land areas. **b**, The model-grid point association among LAI_{NL} term and C_{NL}. Colors
719 indicate area-weighted model-grid point average change in nonlinear canopy partitioning $(C/P)_{NL}$ in
720 percentage points (pp). **c**, The inter-model association among 4xCO2 changes in total canopy throughfall,
721 calculated as the difference between WY precipitation and WY leaf evaporation ($P\text{-}E_L$, mm WY^{-1}) and
722 total runoff (mm WY^{-1}) in the COU run. **d**, As in **b**, except showing the model-grid point association
723 among precipitation throughfall, runoff, and runoff partitioning (colors) from the COU run. **e**, The inter-
724 model association among the C_{NL} (mm WY^{-1}) and the nonlinear soil water flux (S_{NL}, mm WY^{-1}). **f**, as in **b**
725 and **d**, but showing the model-grid point association between C_{NL} and S_{NL}. Colors indicate the nonlinear
726 soil partitioning, $(S/P)_{NL}$. In **a**, **c**, and **e**, R-squared and p-values are reported. Model numbers are the same
727 as presented in **Figure 4-6**. In **b**, **d**, and **e**, red text indicates the percentage of pooled model-grid points
728 falling into that quadrant.

729 In contrast to the canopy water flux from plant-based ET, there is little nonlinearity
730 that emerges in runoff partitioning or runoff itself, and—where it exists—it tends to be
731 negative or statistically insignificant, implying that interactions among the RAD and BGC

weakly reduce runoff (e.g., **Figs. 9h, 12k-m**). Because there is not a strong nonlinear runoff term to explain, we instead focus on the factors determining total runoff in the fully-coupled COU run (**Fig. 13c,d**). While the assumption has always been that plant-driven runoff enhancements were conditioned on precipitation changes, precipitation, not plants, is the dominant factor shaping runoff changes across the ensemble, even in the BGC run where plant effects are thought to be central to hydrologic changes (**Fig. 11-13**). The result here is consistent with other work that shows that, even in the BGC run alone, precipitation changes are five times more important than transpiration changes for determining runoff changes (Lesk et al. 2025). Nonlinear vegetation responses do appear to impact runoff responses in regions with precipitation decreases, reducing runoff partitioning or countering any runoff partitioning gains from the BGC run (**Fig. 11f,** pink line). This implies that in the models, plants take their share of precipitation regardless of precipitation change, which in turn cuts into the runoff allocation where precipitation is limited. In contrast, runoff appears to increase primarily through increased precipitation (**Figs. 12e,l**) and canopy throughfall, with the latter estimated as the difference between precipitation and leaf evaporation (**Fig. 13c, d**).

The relationship between throughfall, runoff, and runoff partitioning is clear at both the inter-model and model grid-point scales, as enhanced throughfall increases runoff (**Figs. 13c, d**). As such, in regions where increased runoff partitioning does occur, these changes are associated with precipitation changes that more than compensate for canopy interception and leaf evaporation changes, or have larger increases in extreme precipitation relative to other regions (**Fig. S4**). For example, changes in extreme precipitation changes (defined as the maximum total precipitation (mm) occurring over a five-day period in each WY) in $\Delta(Q/P)$ positive regions are 50% larger than in $\Delta(C/P)$ positive regions, driven by a strong radiative response in those regions (**Fig. S4d,e**). This is consistent with earlier work that showed that the strength of extreme precipitation change accounts for the strength of runoff partitioning changes in models (Mankin et al. 2018).

We find that plant changes due to interactions of the RAD and BGC runs act to draw down soil water, drying the surface (**Fig. 13e-f**). Global-scale inter-model decreases in S_{NL} are tightly associated with increases in C_{NL} (**Fig. 13e**). The result implies that the increase in plant-based ET (e.g., **Fig. 13a,b**) comes at the expense of soil water. This relationship holds across grid points and models, as positive C_{NL} is associated with decreases in $(S/P)_{NL}$ (colors in **Fig. 13f**). This implies that the strength of the greening and drying pattern in the CMIP6

ensemble (**Fig. 1)** is, in part, a function of the nonlinear increase in plant growth and the associated increase in plant-based ET, which leads to soil water reductions in the CMIP6 ensemble.

4. Discussion & Conclusions

Relative to the CMIP5, the latest generation of CMIP6 ESMs simulate larger interactions between the radiative and biogeochemical effects of [CO_2] (Huang et al. 2022) (**Fig. 4**). There are a number of potential reasons for the growth in these interactions, from varied sophistication in nutrient cycling schemes, mortality, disturbance, and succession, among others. Irrespective of the precise reasons for these emergent interactions between the radiative and biogeochemical effects of CO_2, they lead to larger and more uncertain nonlinear terms in plant growth and net ecosystem exchange that are associated with a reduced sensitivity of the land carbon feedbacks to warming across the ensemble (**Fig. 5**). These plant responses have consequences for hydrology (**Figs. 8-13**): leaf areas increase beyond what would be predicted by the sum of CO_2 fertilization and radiative effects alone, leading to *increased* ecosystem water use, both absolutely (as total plant-based ET increases) (**Fig. 8**) and relatively (as plant-based ET comprises an increasing fraction of precipitation) (**Fig. 9**). These increases in plant-based ET from interactions among RAD and BGC contribute to land-surface drying (**Figs. 11-12**) or counter any gains from increased ecosystem WUE. Vegetation in CMIP6 simulations only increases water availability when comparing radiative and biogeochemical simulations in isolation (Swann et al. 2016; Scheff et al. 2021). When radiative and biogeochemical responses can interact in simulations as they do in the real world, the models suggest that vegetation and its water use counter (or exceed) any increases in runoff or soil moisture from stomatal closure in the BGC runs. In the fully coupled simulations, plants and their responses to [CO_2] generally dry the land.

These results suggest that the curious global pattern of vegetation greening and land surface drying (Mankin et al. 2017a) projected by the models appear to be internally consistent, meaning that the soil drying is, in part, associated with enhanced greening (**Figs. 1, 13**). It does not suggest, however, that they are reflective of what will occur in the real world. Future investigations should consider the set of processes governing carbon uptake and release by the land (**Fig. 6**), and how this has evolved across the CMIP5 to CMIP6 ensemble and whether this has contributed to a weaker climate-carbon feedback (**Fig. 5b**).

That nonlinear interactions among nutrient cycles and warming has emerged in the models is not surprising (Burkett et al. 2005; Field et al. 1995, 2007). It is also not surprising that the magnitude of and uncertainty in such interactions has increased across model generations even as the models become more realistic (Fisher and Koven 2020; Zaehle et al. 2015). However, the emergence of sizable nonlinear interactions in carbon feedbacks appears to be a new feature of the latest generation of CMIP relative to earlier generations (e.g., **Fig. 4**) (Huang et al. 2022). While new parameterizations likely make land surface schemes more reflective of real-world processes, how they interact to shape model responses and accuracy requires continued evaluation. Certainly, in this instance, the CMIP6 range in the magnitude of nonlinear carbon responses has increased relative to CMIP5, and the reasons for this change are a worthy subject for future research.

Our findings reinforce a more widespread need for the perturbed parameter ensembles being pursued by researchers in the land surface modeling community (Zarakas et al. 2024; McNeall et al. 2024). As science seeks to understand the independent and interactive effects of these parametrizations schemes around plants, nutrients, and hydrology, such interactions can give very different model answers, even within the same land surface model (Zarakas et al. 2020, 2024). Our results here emphasize a point relevant to these efforts: one-at-a-time perturbed parameter ensembles, while computationally feasible, may actually be insufficient to characterize the importance of any one land surface parameter, owing to interactive effects. Instead, "global variance-based" sensitivity analyses (Saltelli 2000; Saltelli et al. 2010) should be pursued, where modelers jointly and independently perturb carbon, plant, and water parameters to evaluate not just the contribution of any one parameter to the distribution of model answers, but how interactions among parameters influence uncertainties in model responses. These ensembles could help identify the parameters most culpable for uncertainty in RAD and BGC interactions and position their benchmarking to the real world.

As ESMs incorporate more sophisticated processes (Fisher and Koven 2020), nonlinearities are emerging with hydrologic consequences. Furthermore, considerable model spread in land carbon and hydrology stem from model representations of phenology, nutrient limitations, soil microbial and respiratory processes, vegetation mortality from wildfire, insects and pathogens, drought stress, wind storms, and post-disturbance successional processes (Ziehn et al. 2021; Sanderson and Fisher 2020; Albrich et al. 2020; Trugman et al. 2018; Zaehle et al. 2015; Fisher and Koven 2020). To realistically represent the land carbon

sink and its implications for water availability for people and ecosystems, model development is rightfully focused on improving representation of the soil water-plant-atmosphere continuum (Clark et al. 2015) and plant mortality and succession (Anderegg et al. 2013; Trugman et al. 2018; Williams et al. 2022). To what extent these processes collectively generate nonlinear feedbacks in the real world is poorly understood and must be evaluated. At the same time, greater model sophistication may improve the realism of any one model, it may also give rise to additional poorly understood nonlinear feedbacks, which may, or may not, be reflective of the real world. Identification of these nonlinearities and their consequences, as we have done here, is an essential step and creates a scientific imperative to understand the properties of the emerging nonlinearities in state-of-the-art ESMs.

Acknowledgments.

We acknowledge the Earth System Grid Federation and their archiving of the Coupled Model Intercomparison Project (Phase 6) data. We thank Dartmouth's Research Computing, which provided computational support, as well as Naomi Henderson and H. Liu for data serving support in the Division of Ocean and Climate Physics at Lamont-Doherty Earth Observatory of Columbia University. We thank Y. Huang (CSIRO) and V. Arora (CCMA) for sharing additional details of the feedback parameter calculations. We thank two reviewers (including V. Arora) for their contributions to improving this work, as well as the participants of the Carnegie Trust-funded workshop on "Continental Climate Change: Simple Models to Understand the Future" held at University of St. Andrews for providing feedback on this work. We acknowledge funding from NOAA MAPP NA20OAR4310425 (J.S.M, R.S., J.E.S., and Z.L); DOE DESC0022302 (J.S.M, B.I.C, R.S., A.P.W. and J.E.S.); FRQNT 31916 (C. L.); NSF CLD 2304953 (J.S.M); the Gordon and Betty Moore Foundation 11974 (A.P.W.); and the Neukom Institute for Computational Science (J.S.M., C.L., and E.D.M.) and the Rockefeller Center at Dartmouth (J.S.M.).

Data Availability Statement.

All CMIP5 and CMIP6 C4MIP data that support this study are publicly available at: https://esgf-node.llnl.gov/. All code that supports this study will be made available upon reasonable request.

858

859 REFERENCES

860 Albrich, K., W. Rammer, M. G. Turner, Z. Ratajczak, K. H. Braziunas, W. D. Hansen, and R.
861 Seidl, 2020: Simulating forest resilience: A review. *Global Ecology and*
862 *Biogeography*, **29**, 2082–2096, https://doi.org/10.1111/geb.13197.

863 Anderegg, W. R. L., J. Kane, and L. D. L. Anderegg, 2013: Consequences of widespread tree
864 mortality triggered by drought and temperature stress. *Nature Climate Change*, **3**, 30–
865 30, https://doi.org/10.1038/NCLIMATE1635.

866 Arora, V. K., and Coauthors, 2020: Carbon–concentration and carbon–climate feedbacks in
867 CMIP6 models and their comparison to CMIP5 models. *Biogeosciences*, **17**, 4173–
868 4222, https://doi.org/10.5194/bg-17-4173-2020.

869 Aston, A. R., 1984: The effect of doubling atmospheric CO2 on streamflow: A simulation.
870 *Journal of Hydrology*, **67**, 273–280, https://doi.org/10.1016/0022-1694(84)90246-4.

871 Betts, R. A., and Coauthors, 2007: Projected increase in continental runoff due to plant
872 responses to increasing carbon dioxide. *Nature*, **448**, 1037–1041,
873 https://doi.org/10.1038/nature06045.

874 Bonan, G. B., M. Williams, R. A. Fisher, and K. W. Oleson, 2014: Modeling stomatal
875 conductance in the earth system: linking leaf water-use efficiency and water transport
876 along the soil–plant–atmosphere continuum. *Geoscientific Model Development*, **7**,
877 2193–2222, https://doi.org/10.5194/gmd-7-2193-2014.

878 Burkett, V. R., and Coauthors, 2005: Nonlinear dynamics in ecosystem response to climatic
879 change: Case studies and policy implications. *Ecological Complexity*, **2**, 357–394,
880 https://doi.org/10.1016/j.ecocom.2005.04.010.

881 Canadell, J.G., Monteiro, P.M.S., Costa, M.H., Cotrim da Cunha, L., Cox, P.M., Eliseev,
882 A.V., Henson, S., and Ishii, M., 2021: Global Carbon and other Biogeochemical
883 Cycles and Feedbacks. *Climate Change 2021: The Physical Science Basis.*
884 *Contribution of Working Group I to the Sixth Assessment Report of the*
885 *Intergovernmental Panel on Climate Change [Masson-Delmotte, V., P. Zhai, A.*
886 *Pirani, S.L. Connors, C. Péan, S. Berger, N. Caud, Y. Chen, L. Goldfarb, M.I. Gomis,*
887 *M. Huang, K. Leitzell, E. Lonnoy, J.B.R. Matthews, T.K. Maycock, T. Waterfield, O.*
888 *Yelekçi, R. Yu, and B. Zhou (eds.)]. doi: 10.1017/9781009157896.007*, Cambridge
889 University Press, 673-816,.

890 Clark, M. P., and Coauthors, 2015: Improving the representation of hydrologic processes in
891 Earth System Models. *Water Resources Research*, **51**, 5929–5956,
892 https://doi.org/10.1002/2015WR017096.

893 Cook, B. I., J. S. Mankin, K. Marvel, A. P. Williams, J. E. Smerdon, and K. J. Anchukaitis,
894 2020: Twenty-First Century Drought Projections in the CMIP6 Forcing Scenarios.
895 *Earth's Future*, **8**, e2019EF001461, https://doi.org/10.1029/2019EF001461.

——, ——, A. P. Williams, K. D. Marvel, J. E. Smerdon, and H. Liu, 2021: Uncertainties, Limits, and Benefits of Climate Change Mitigation for Soil Moisture Drought in Southwestern North America. *Earth's Future*, **9**, e2021EF002014, https://doi.org/10.1029/2021EF002014.

Cowan, I. R., and G. D. Farquhar, 1977: Stomatal function in relation to leaf metabolism and environment. *Integration of Activity in the Higher Plant*, Cambridge University Press, p. 18.

Cox, P. M., D. Pearson, B. B. Booth, P. Friedlingstein, C. Huntingford, C. D. Jones, and C. M. Luke, 2013: Sensitivity of tropical carbon to climate change constrained by carbon dioxide variability. *Nature*, **494**, 341–344, https://doi.org/10.1038/nature11882.

Davies-Barnard, T., and Coauthors, 2020: Nitrogen cycling in CMIP6 land surface models: progress and limitations. *Biogeosciences*, **17**, 5129–5148, https://doi.org/10.5194/bg-17-5129-2020.

De Kauwe, M. G., and Coauthors, 2013: Forest water use and water use efficiency at elevated CO2: A model-data intercomparison at two contrasting temperate forest FACE sites. *Global Change Biology*, **19**, 1759–1779, https://doi.org/10.1111/gcb.12164.

Eyring, V., S. Bony, G. A. Meehl, C. A. Senior, B. Stevens, R. J. Stouffer, and K. E. Taylor, 2016: Overview of the Coupled Model Intercomparison Project Phase 6 (CMIP6) experimental design and organization. *Geoscientific Model Development*, **9**, 1937–1958, https://doi.org/10.5194/gmd-9-1937-2016.

Felzer, B. S., T. W. Cronin, J. M. Melillo, D. W. Kicklighter, and C. A. Schlosser, 2009: Importance of carbon-nitrogen interactions and ozone on ecosystem hydrology during the 21st century. *Journal of Geophysical Research: Biogeosciences*, **114**, https://doi.org/10.1029/2008JG000826.

Field, C. B., R. B. Jackson, and H. A. Mooney, 1995: Stomatal responses to increased CO2: implications from the plant to the global scale. *Plant, Cell & Environment*, **18**, 1214–1225, https://doi.org/10.1111/j.1365-3040.1995.tb00630.x.

Field, C. B., D. B. Lobell, H. A. Peters, and N. R. Chiariello, 2007: Feedbacks of Terrestrial Ecosystems to Climate Change. *Annual Review of Environment and Resources*, **32**, 1–29, https://doi.org/10.1146/annurev.energy.32.053006.141119.

Fisher, R. A., and C. D. Koven, 2020: Perspectives on the Future of Land Surface Models and the Challenges of Representing Complex Terrestrial Systems. *Journal of Advances in Modeling Earth Systems*, **12**, e2018MS001453, https://doi.org/10.1029/2018MS001453.

Fowler, M. D., G. J. Kooperman, J. T. Randerson, and M. S. Pritchard, 2019: The effect of plant physiological responses to rising CO2 on global streamflow. *Nature Climate Change*, **9**, 873–879, https://doi.org/10.1038/s41558-019-0602-x.

Friedlingstein, P., and Coauthors, 2006: Climate-Carbon Cycle Feedback Analysis: Results from the C4MIP Model Intercomparison. *Journal of Climate*, **19**, 3337–3353.

935 Fung, Inez, Rayner, Peter, and Friedlingstein, Pierre, 2000: Full-Form Earth System Models:
936 Coupled Carbon-Climate Interaction Experiment (the “Flying Leap”). *IGBP*
937 *Newsletter*, **41**.

938 Gottlieb, A. R., and J. S. Mankin, 2024: Evidence of human influence on Northern
939 Hemisphere snow loss. *Nature*, **625**, 293–300, https://doi.org/10.1038/s41586-023-
940 06794-y.

941 Hall, A., P. Cox, C. Huntingford, and S. Klein, 2019: Progressing emergent constraints on
942 future climate change. *Nature Climate Change*, **9**, 269–278,
943 https://doi.org/10.1038/s41558-019-0436-6.

944 Huang, Y., Y.-P. Wang, and T. Ziehn, 2022: Nonlinear interactions of land carbon cycle
945 feedbacks in Earth System Models. *Global Change Biology*, **28**, 296–306,
946 https://doi.org/10.1111/gcb.15953.

947 Idso, S. B., and A. J. Brazel, 1984: Rising atmospheric carbon dioxide concentrations may
948 increase streamflow. *Nature*, **312**, 51–53, https://doi.org/10.1038/312051a0.

949 Jasechko, S., 2018: Plants turn on the tap. *Nature Clim Change*, **8**, 562–563,
950 https://doi.org/10.1038/s41558-018-0212-z.

951 Jones, C. D., and Coauthors, 2016: C4MIP-The Coupled Climate-Carbon Cycle Model
952 Intercomparison Project: Experimental protocol for CMIP6. *Geoscientific Model*
953 *Development*, **9**, 2853–2880, https://doi.org/10.5194/gmd-9-2853-2016.

954 Keenan, D. Y. Hollinger, G. Bohrer, D. Dragoni, J. W. Munger, H. P. Schmid, and A. D.
955 Richardson, 2013: Increase in forest water-use efficiency as atmospheric carbon
956 dioxide concentrations rise. *Nature*, **499**, 324–327,
957 https://doi.org/10.1038/nature12291.

958 Keenan, T. F., and Coauthors, 2023: A constraint on historic growth in global photosynthesis
959 due to rising CO2. *Nat. Clim. Chang.*, **13**, 1376–1381,
960 https://doi.org/10.1038/s41558-023-01867-2.

961 Lee, E., B. S. Felzer, and Z. Kothavala, 2013: Effects of nitrogen limitation on hydrological
962 processes in CLM4-CN. *Journal of Advances in Modeling Earth Systems. Model.*
963 *Earth Syst*, **5**, 741–754, https://doi.org/10.1002/jame.20046.

964 Lehner, F., A. W. Wood, J. A. Vano, D. M. Lawrence, M. P. Clark, and J. S. Mankin, 2019:
965 The potential to reduce uncertainty in regional runoff projections from climate
966 models. *Nature Climate Change*, **9**, 926–933, https://doi.org/10.1038/s41558-019-
967 0639-x.

968 Lemordant, L., P. Gentine, A. S. Swann, B. I. Cook, and J. Scheff, 2018: Critical impact of
969 vegetation physiology on the continental hydrologic cycle in response to increasing
970 CO2. *Proceedings of the National Academy of Sciences*, **0**, 2–7,
971 https://doi.org/10.1073/pnas.1720712115.

Lesk, C. S., J. M. Winter, and J. S. Mankin, 2025: Projected runoff declines from plant physiological effects on precipitation. *Nat Water*, **3**, 167–177, https://doi.org/10.1038/s44221-024-00361-z.

Leung, and Coauthors, 2023: Ch. 3. Earth systems processes. *Fifth National Climate Assessment. Crimmins, A.R., C.W. Avery, D.R. Easterling, K.E. Kunkel, B.C. Stewart, and T.K. Maycock, Eds. U.S. Global Change Research Program, Washington, DC, USA. https://doi.org/10.7930/NCA5.2023.CH3*, U.S. Global Change Research Program, Washington, DC, 1–470.

Liu, L., P. Ciais, M. Wu, R. S. Padrón, P. Friedlingstein, J. Schwaab, L. Gudmundsson, and S. I. Seneviratne, 2023: Increasingly negative tropical water–interannual CO2 growth rate coupling. *Nature*, **618**, 755–760, https://doi.org/10.1038/s41586-023-06056-x.

Mankin, J. S., J. E. Smerdon, B. I. Cook, A. P. Williams, and R. Seager, 2017a: The curious case of projected Twenty-First-Century Drying but Greening in the American West. *Journal of Climate*, **30**, 8689–8710, https://doi.org/10.1175/JCLI-D-17-0213.1.

——, D. Viviroli, M. M. Mekonnen, A. Y. Hoekstra, R. M. Horton, J. E. Smerdon, and N. S. Diffenbaugh, 2017b: Influence of internal variability on population exposure to hydroclimatic changes. *Environmental Research Letters*, **12**, https://doi.org/10.1088/1748-9326/aa5efc.

——, R. Seager, J. E. Smerdon, B. I. Cook, A. P. Williams, and R. M. Horton, 2018: Blue Water Trade-Offs With Vegetation in a CO2-Enriched Climate. *Geophysical Research Letters*, **45**, 3115–3125, https://doi.org/10.1002/2018GL077051.

——, ——, ——, ——, and ——, 2019: Mid-latitude freshwater availability reduced by projected vegetation responses to climate change. *Nature Geoscience*, https://doi.org/10.1038/s41561-019-0480-x.

McNeall, D., E. Robertson, and A. Wiltshire, 2024: Constraining the carbon cycle in JULES-ES-1.0. *Geoscientific Model Development*, **17**, 1059–1089, https://doi.org/10.5194/gmd-17-1059-2024.

Medlyn, B. E., and Coauthors, 2011: Reconciling the optimal and empirical approaches to modelling stomatal conductance. *Global Change Biology*, **17**, 2134–2144, https://doi.org/10.1111/j.1365-2486.2010.02375.x.

Milly, P. C. D., and K. A. Dunne, 2016: Potential evapotranspiration and continental drying. *Nature Climate Change*, **6**, 946–949, https://doi.org/10.1038/NCLIMATE3046.

Roderick, M. L., P. Greve, and G. D. Farquhar, 2015: On the assessment of aridity with changes in atmospheric CO2. *Water Resources Research*, **51**, 5450–5463, https://doi.org/10.1002/2015WR017031.

Sabot, M. E. B., and Coauthors, 2022: One Stomatal Model to Rule Them All? Toward Improved Representation of Carbon and Water Exchange in Global Models. *Journal of Advances in Modeling Earth Systems*, **14**, e2021MS002761, https://doi.org/10.1029/2021MS002761.

1011 Saltelli, A., 2000: What is Sensitivity Analysis? *Sensitivity Analysis*, 3–13.

1012 ——, P. Annoni, I. Azzini, F. Campolongo, M. Ratto, and S. Tarantola, 2010: Variance based
1013 sensitivity analysis of model output. Design and estimator for the total sensitivity
1014 index. *Computer Physics Communications*, **181**, 259–270,
1015 https://doi.org/10.1016/j.cpc.2009.09.018.

1016 Sanderson, B. M., and R. A. Fisher, 2020: A fiery wake-up call for climate science. *Nat.*
1017 *Clim. Chang.*, **10**, 175–177, https://doi.org/10.1038/s41558-020-0707-2.

1018 Scheff, J., J. S Mankin, S. Coats, and H. Liu, 2021: CO2-plant effects do not account for the
1019 gap between dryness indices and projected dryness impacts in CMIP6 or CMIP5.
1020 *Environmental Research Letters*, **16**, 034018, https://doi.org/10.1088/1748-
1021 9326/abd8fd.

1022 Skinner, C. B., and Coauthors, 2017: The role of plant CO2 physiological forcing in shaping
1023 future daily-scale precipitation. *Journal of Climate*, JCLI-D-16-0603.1,
1024 https://doi.org/10.1175/JCLI-D-16-0603.1.

1025 Sokolov, A. P., D. W. Kicklighter, J. M. Melillo, B. S. Felzer, C. A. Schlosser, and T. W.
1026 Cronin, 2008: Consequences of Considering Carbon–Nitrogen Interactions on the
1027 Feedbacks between Climate and the Terrestrial Carbon Cycle. *Journal of Climate*, **21**,
1028 3776–3796, https://doi.org/10.1175/2008JCLI2038.1.

1029 Swann, A. L. S., F. M. Hoffman, C. D. Koven, and J. T. Randerson, 2016: Plant responses to
1030 increasing CO2 reduce estimates of climate impacts on drought severity. *Proceedings*
1031 *of the National Academy of Sciences*, **113**, 10019–10024,
1032 https://doi.org/10.1073/pnas.1604581113.

1033 Thornton, P. E., and Coauthors, 2009: Carbon-nitrogen interactions regulate climate-carbon
1034 cycle feedbacks: results from an atmosphere–ocean general circulation model.
1035 *Biogeosciences*, **6**, 2099–2120, https://doi.org/10.5194/bg-6-2099-2009.

1036 Trugman, A. T., D. Medvigy, J. S. Mankin, and W. R. L. L. Anderegg, 2018: Soil moisture
1037 drought as a major driver of carbon cycle uncertainty. *Geophysical Research Letters*,
1038 **45**, 6495–6503, https://doi.org/10.1029/2018GL078131.

1039 Vitousek, P. M., and R. W. Howarth, 1991: Nitrogen limitation on land and in the sea: How
1040 can it occur? *Biogeochemistry*, **13**, 87–115, https://doi.org/10.1007/BF00002772.

1041 Wenzel, S., P. M. Cox, V. Eyring, and P. Friedlingstein, 2014: Emergent constraints on
1042 climate-carbon cycle feedbacks in the CMIP5 Earth system models. *Journal of*
1043 *Geophysical Research: Biogeosciences*, **119**, 794–807,
1044 https://doi.org/10.1002/2013JG002591.Received.

1045 Williams, A. P., and Coauthors, 2022: Growing impact of wildfire on western US water
1046 supply. *PNAS*, **119**, https://doi.org/10.1073/pnas.2114069119.

1047 Yang, Y., M. L. Roderick, S. Zhang, T. R. Mcvicar, and R. J. Donohue, 2019: Hydrologic
1048 implications of vegetation response to elevated CO 2 in climate projections. *Nature*
1049 *Climate Change*, **9**, 44–49, https://doi.org/10.1038/s41558-018-0361-0.

Zaehle, S., 2013: Terrestrial nitrogen–carbon cycle interactions at the global scale. *Philosophical Transactions of the Royal Society B: Biological Sciences*, **368**, 20130125, https://doi.org/10.1098/rstb.2013.0125.

Zaehle, S., P. Friedlingstein, and A. D. Friend, 2010: Terrestrial nitrogen feedbacks may accelerate future climate change. *Geophysical Research Letters*, **37**, L01401, https://doi.org/10.1029/2009GL041345.

——, C. D. Jones, B. Houlton, J.-F. Lamarque, and E. Robertson, 2015: Nitrogen Availability Reduces CMIP5 Projections of Twenty-First-Century Land Carbon Uptake. *Journal of Climate*, **28**, 2494–2511, https://doi.org/10.1175/JCLI-D-13-00776.1.

Zarakas, C. M., A. L. S. Swann, M. M. Laguë, K. C. Armour, and J. T. Randerson, 2020: Plant Physiology Increases the Magnitude and Spread of the Transient Climate Response to CO2 in CMIP6 Earth System Models. *Journal of Climate*, **33**, 8561–8578, https://doi.org/10.1175/JCLI-D-20-0078.1.

Zarakas, C. M., and Coauthors, 2024: Land Processes Can Substantially Impact the Mean Climate State.

Zhang, J., and Coauthors, 2018: Insights into the Molecular Mechanisms of CO2-Mediated Regulation of Stomatal Movements. *Current Biology*, **28**, R1356–R1363, https://doi.org/10.1016/j.cub.2018.10.015.

Zhou, S., B. Yu, B. R. Lintner, K. L. Findell, and Y. Zhang, 2023: Projected increase in global runoff dominated by land surface changes. *Nat. Clim. Chang.*, 1–8, https://doi.org/10.1038/s41558-023-01659-8.

Ziehn, T., Y.-P. Wang, and Y. Huang, 2021: Land carbon-concentration and carbon-climate feedbacks are significantly reduced by nitrogen and phosphorus limitation. *Environ. Res. Lett.*, **16**, 074043, https://doi.org/10.1088/1748-9326/ac0e62.

Supplemental Material:

Nonlinear carbon feedbacks in CMIP6 and their impacts on future freshwater availability

Justin S. Mankin[a,b], Noel Siegert[a,b], Jason E. Smerdon[b,c], Benjamin I. Cook[b,d], Richard Seager[b], A. Park Williams[e], Corey Lesk[a], Zhiying Li[a], Harmanveer Singh[a,f], & Emily Martinez[a]

[a] *Department of Geography, Dartmouth College, Hanover, NH*

[b] *Lamont-Doherty Earth Observatory of Columbia University, Palisades, NY*

[c] *Columbia Climate School, Columbia University, New York, NY*

[d] *NASA Goddard Institute for Space Studies, New York, NY*

[e] *Department of Geography, UCLA, Los Angeles, CA*

[f] *School of Marine & Atmospheric Sciences, Stony Brook University, Stony Brook, NY*

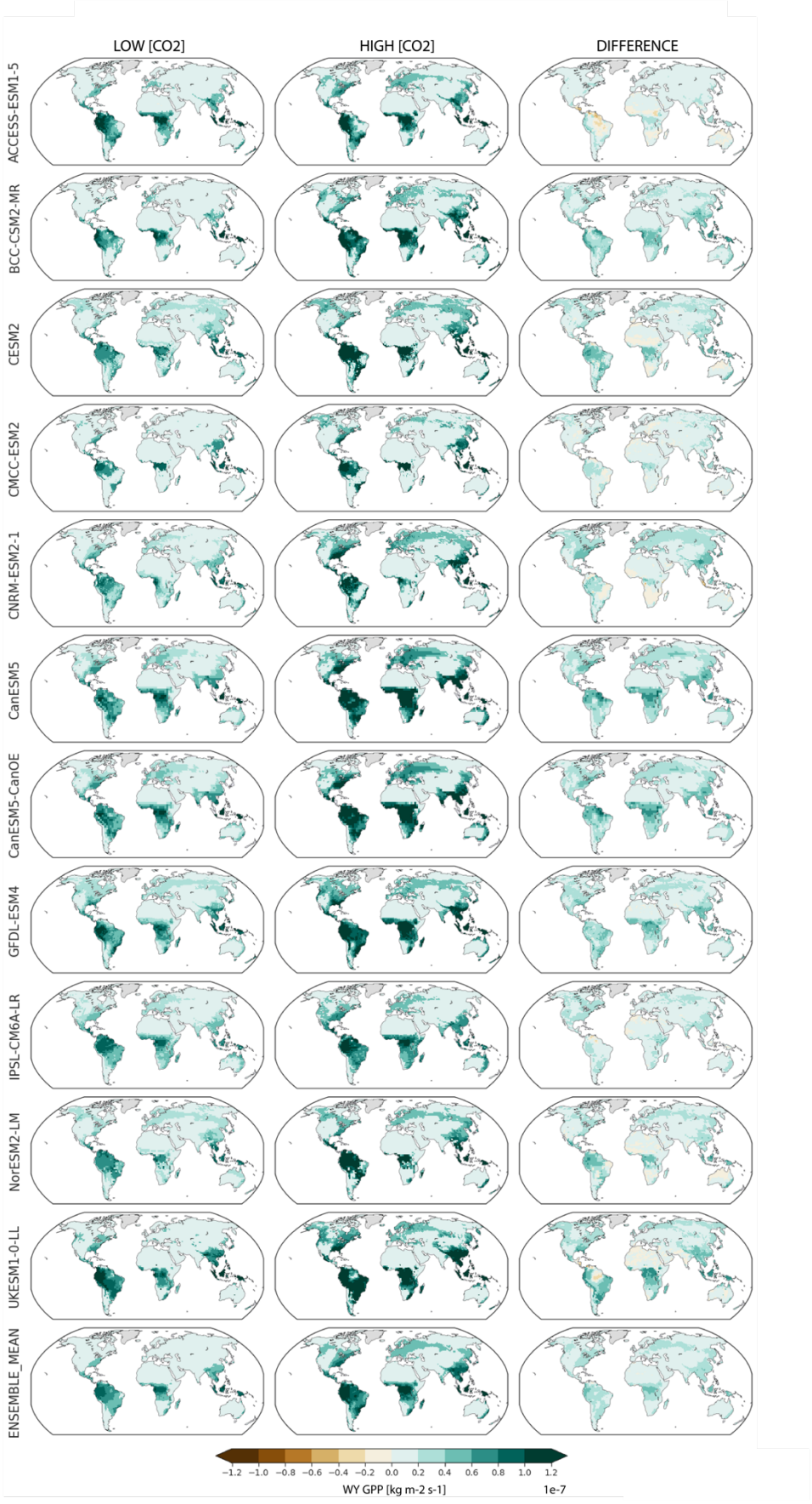

1093 **Fig. S1** Climatological GPP and its change in the 1pctCO2 fully coupled simulation (COU) for each model
1094 in the analysis and the ensemble mean (rows). Columns correspond to the climatological water-year (WY)
1095 mean of GPP in the first 30 years, last 30 years, and difference among the two periods for each simulation.

1096

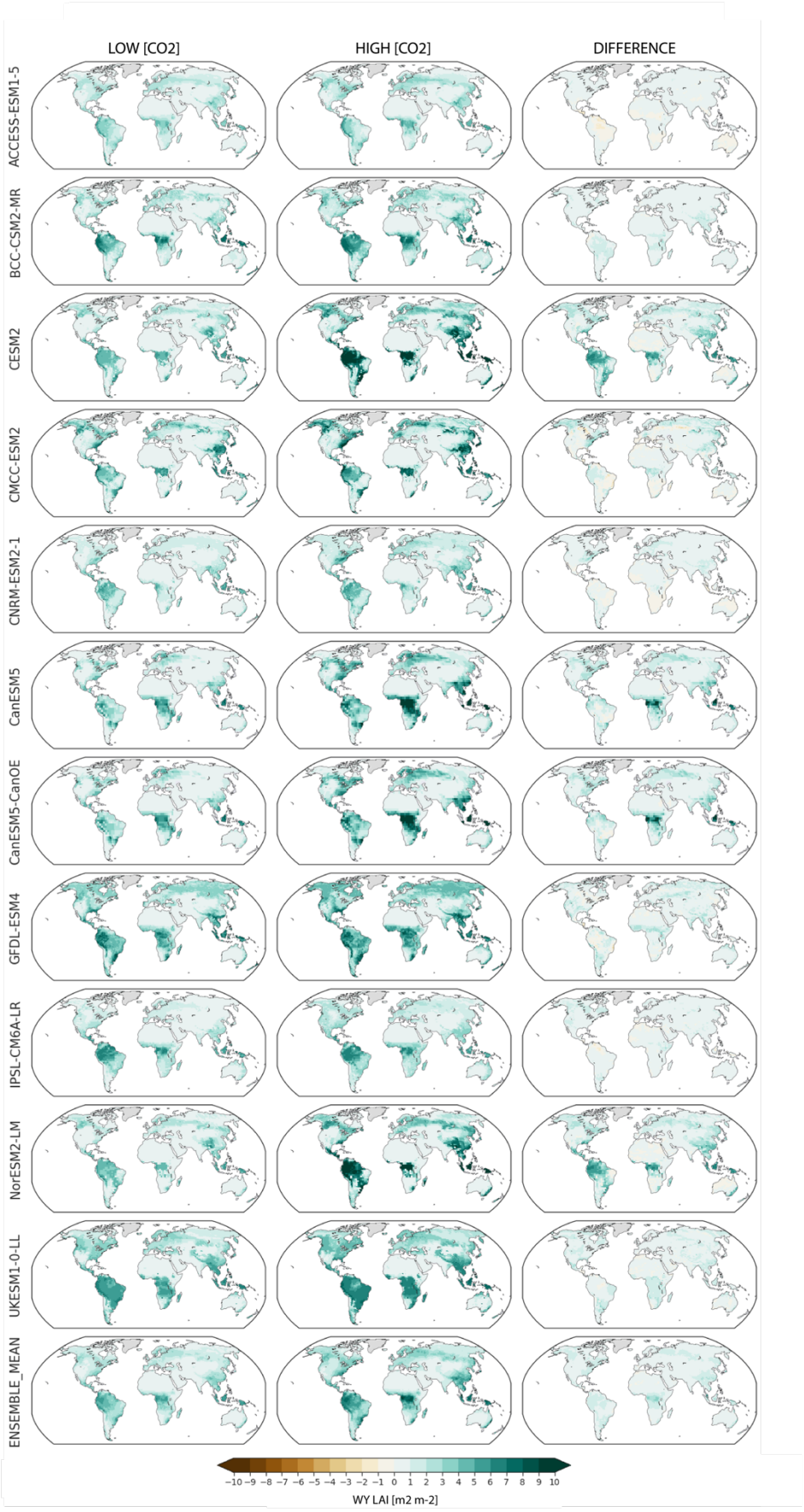
LOW [CO2]
HIGH [CO2]
DIFFERENCE
ACCESS-ESM1-5
BCC-CSM2-MR
CESM2
CMCC-ESM2
CNRM-ESM2-1
CanESM5
CanESM5-CanOE
GFDL-ESM4
IPSL-CM6A-LR
NorESM2-LM
UKESM1-0-LL
ENSEMBLE_MEAN
−10 −9 −8 −7 −6 −5 −4 −3 −2 −1 0 1 2 3 4 5 6 7 8 9 10
WY LAI [m2 m-2]

Fig. S2 Climatological LAI and its change in the 1pctCO2 fully coupled simulation (COU) for each model in the analysis and the ensemble mean (rows). Columns correspond to the climatological water-year (WY) mean of LAI in the first 30 years, last 30 years, and difference among the two periods for each simulation.

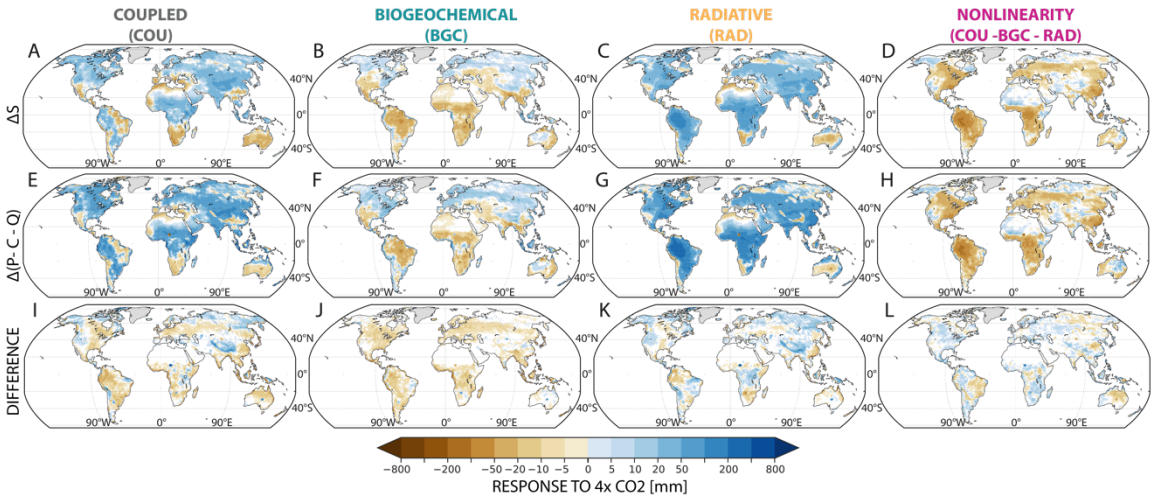

Fig. S3 Climatological water-year (WY) ensemble-mean changes in response to 4xCO2 in the S term in each experiment used in the analysis, defined as the sum of soil evaporation and the first difference of 2-m soil moisture (**a-d**), versus the S term when it is calculated as the residual of the difference between P, C, and Q (**e-h**). The last row (**i-l**) shows the difference between the two estimates of the S term. Only statistically significant changes are shown.

1111

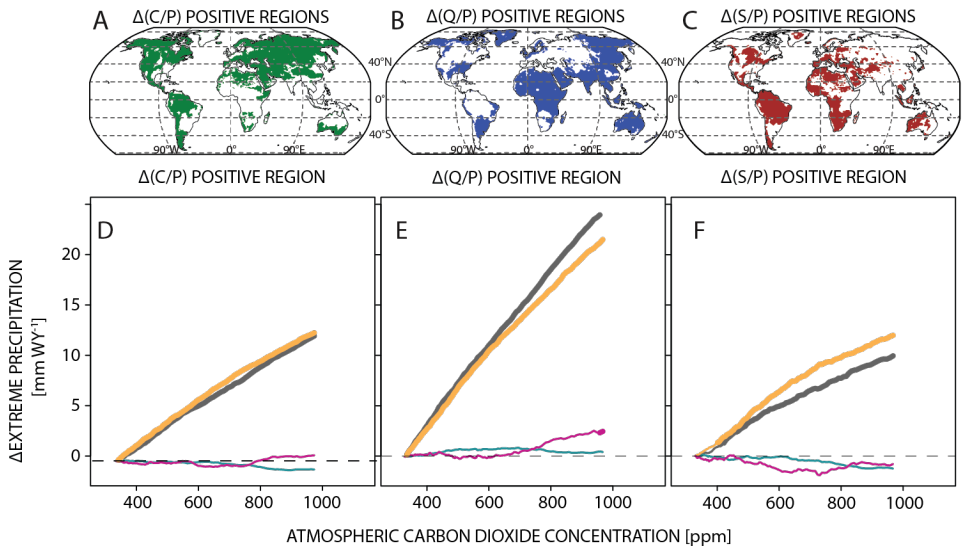

1112

1113 **Fig. S4** Changes in extreme precipitation (**d-f**) as a function of increasing [CO_2] in Δ(C/P), Δ(Q/P), and
1114 Δ(S/P) regions (**a-c**) based on the ensemble-mean of the COU run (see maps in **Fig. 9, a, e, i**). Significance
1115 in the time series is presented as a bolded line where the 30-year rolling ensemble mean change is greater
1116 than one standard deviation of changes across the ensemble at that time.